POLITECNICO DI TORINO

Master of Science

In Environmental Engineering – Climate Change

Thesis

Urban Thermal Hotspots: A Machine Learning Approach to Analyzing Urban Heat Island Dynamics in Stockholm, Sweden

Politecnico di Torino

Supervisors

Prof. Marco Piras
Prof. Zahra Kalantari

Candidate

Ali Gholami

A.A. 2024/2025

Abstract

Urbanization and climate change have posed challenges for managing one of the key concerns in recent years, which is increasing of Urban Heat Islands (UHIs), especially in urban areas. These events can increase risks to human health, buildings and roads, and urban areas in general. The analysis of UHI has been studied in this thesis for both summer and winter months from 2014-2023 using satellite images in Stockholm, Sweden. Key input variables include temperature, Normalized Difference Vegetation Index (NDVI), Normalized Difference Built-up Index (NDBI), Land Surface Albedo (LSA), wind speed, and Local Climate Zones (LCZs). Urban Heat Island maps were created in this study for both summer and winer months. To access the prediction capabilities of machine learning algorithms for UHI, seven machine learning algorithms such as Linear Regression, Support Vector Regression, Decision Tree, K-Nearest Neighbors, Random Forest, Extra Trees, and XGBoost were analysed. Random Forest showed the best-performing result based on R^2, RMSE, and MAE. Feature importance analysis showed NDVI as major contributor to UHI and UHI mitigation, and NDBI were linked to higher UHI intensities.

In the next step, the study focused on a trend-based climate change projection using bias-corrected temperature data approach using the NEX-GDDP-CMIP6 dataset under two different Shared Socioeconomic Pathways (SSPs), SSP1-2.6 and SSP5-8.5, with the help of machine learning algorithms to assess and analyse future UHI trend from 2030-2039, which they showed increasing trends of UHI for both seasons in the coming years.

Acknowledgements

To my supervisors, in Turin and in Stockholm, I am grateful to have you in this work and for your guidance through this journey. Thank you for providing me with valuable insights, help, and providing me the time to discuss every challenge I faced during this period. Thank you for helping me to overcome these challenges again and again.

To myself, for doing my best to achieve this step. To have a strong desire to do my work, dedicated, and ambitious. To capture the experience of this journey with a great enthusiasm.

To my family, who are supporting me during my academic journey, who are beside me for every challenge that I have faced, am facing, and will face. For believing and understanding me in every moment.

A heartfelt thank you to all those who have inspired and taught me. In times of difficulty, know that I have found great comfort in your words and reassurances. Many of you have taken time away from your activities to be able to help me. I hope to give you back what you have given me.

Table of Contents

1. Introduction

One of the most significant ecological issues of concern in a city is the existence of Urban Heat Islands (UHIs). With city growth, so does the UHI effect, where urban temperatures are higher than those in surrounding rural areas. UHIs exist because natural cover is replaced by hard, impervious, and urbanized surfaces such as concrete and asphalt and other human-made materials. These materials retain heat during the day from the sun, and at night when they cool down, instead of releasing the heat energy absorbed during the day, it is emitted slowly; both situations cause increased temperatures in both day and night. Ultimately, the effects of urban heat islands lead to altered subsequent energy consumption, air quality, public health, and even quality of life (Heaviside et al., 2017; Magli et al., 2015; Sarrat et al., 2006).

Green infrastructure can help to reduce the intensity of UHIs. These infrastructures like parks, urban forests, green roofs, green walls are effective for cool down the temperature in urban areas, in a way that if we increase them, they help to reduce surface and air temperatures by improving shading and affecting evapotranspiration. They offer a strong approach to mitigate the effects of UHI. Climate change can increase UHI effects since climate change can affect by increasing global temperatures and consequently more heatwaves, which can lead to rising temperatures in cities and urban areas so it is important to take into account climate change to analyse future UHIs. By working on climate projections this thesis can provide long term UHI trend under different climate change scenarios. This work is important for urban planners since it is helpful to improve resilience to future climate conditions.

The main objective of this work is to analyse the intensity of UHIs in summer and winter seasons for the past 10 years (2014-2023), with purpose:

- To analyse UHI intensity and creation of UHI intensity maps for each month of the both summer and winter seasons (3 months of summer and 3 months of winter).

- Using machine learning (ML) techniques such as Linear Regression, Support Vector Regression (SVR), Decision Tree, K-Nearest Neighbors (KNN), Random Forest, Extra Trees, and XGBoost to predict UHI intensity.
- To Assess how machine learning algorithms perform, and to see the most accurate one using RMSE, R^2, and MAE.
- Identify the regions, which are more critical in terms of UHI by using an intensity classification of the UHI maps created before.
- Analyse the UHI in different Local Climate Zones (LCZs) and see which LCZs have more UHI intensity.
- Projection of UHI trends for next ten years (2030-2039).

This thesis has been worked under the mobility program with the collaboration between KTH Royal Institute of Technology in Stockholm, Sweden and Politecnico di Torino. The time in KTH played an important role of the research methodology and analysis of this work. During the mobility period, KTH provided valuable helps for applying machine learning methods and how to process and interpret climate datasets from the NEX-GDDP-CMIP6 database. The collaboration also helped to access the local data for this thesis as the study area for this work was Stockholm.

In the first chapter, the UHI is explained, what is the UHI, what is the original concept, and its fundamental. Then the focus shifts to the dynamic, UHI impacts, and mitigation. In the next chapter, we talk about the case study, the dataset, the machine learning algorithms, and what are the metrics to evaluate these algorithms. At the final stage of this chapter, we talk about NEX-GDDP-CMIP6 database, and climate change projection scenarios. The results of these analyses are then presented in the next chapter (chapter 4), we see the local climate zone mapping, the UHI analysis in the study period (2014-2023), how ML algorithms performed, and the trend analysis of UHI projection. In the fifth chapter, we discuss about the UHI seasonal

change, what are the impacts of this event in cold cities, and the challenges and opportunities it may propose. Then at the last part of this chapter, we focus on the mitigation strategies for UHI events. In the last chapter, which is the conclusion, we talk about the overall results of this thesis, what are the achievements, and what can be done better or more for more in-depth results.

2. Introduction to Urban Heat Island (UHI)

The Urban Heat Island (UHI) effect and its factors was discovered by Howard in 1818, and since then, the causes and effects of such a phenomenon have been thoroughly explored. UHIs are generally categorized into surface or air temperature UHIs; the surface UHI registers higher temperatures through surface, and the air temperature UHI accounts for the increase in ambient air temperatures due to the heat given off buildings and the subsequent anthropogenic interventions such as cars, factories, and air conditioning units. Therefore, the surface UHI compounds the air temperature UHI, which also adds another thermal burden to an already urbanized environment (*Figure. 1*).

“The temperature of the city is not to be considered as that of the climate”; Luke Howard, which can be translated to the fact that there is an increase temperature that the nature is not responsible for. In his analysis, he stated four different events that make this temperature difference:

1. Human activities that generate heat contribute to the warming of the atmosphere, especially during the winter season.
2. The geometry of urban surfaces which ‘traps’ radiation and obstructs ‘free radiation to the sky.
3. The unevenness of urban surfaces can hinder the movement of the “gentle” summer winds.
4. The availability of moisture for evaporation in the country.

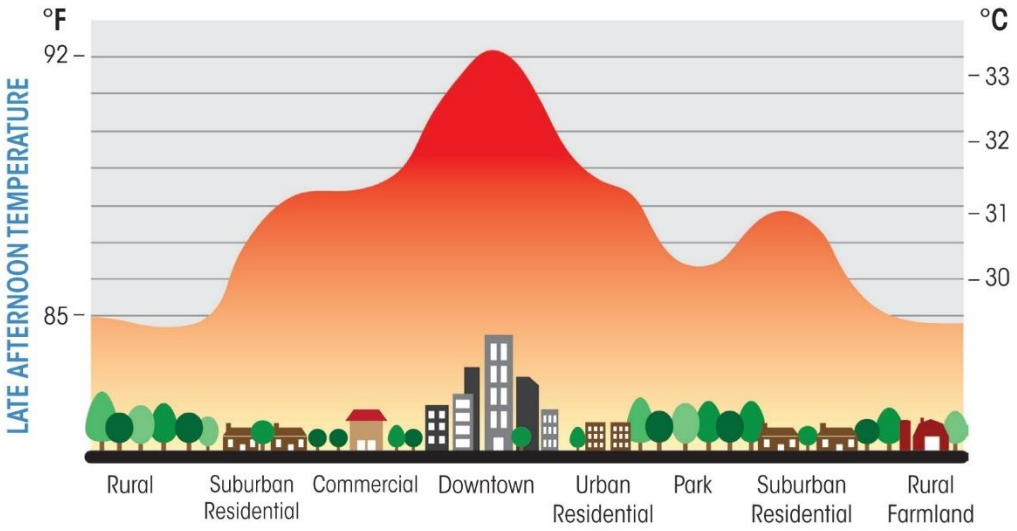

Figure. 1 Urban Heat Island[1]

According to Oke's study (1982), UHIs can be generalised, initially, by the illustration of common features of heat island morphology, describing the *"near-surface"* of the heat island, moreover, he considers irrelevant the topography of the surroundings and puts the accents to the urban/rural boundaries that follows the outline of the built-up area.

Across of the majority of the urban area, the horizontal thermal gradient exhibits a more gradual trend. However, warm spots can sometimes be found in high-density areas such as residential complexes, industrial zones, or downtown, and cool spots can be found in low-density areas such as parks or lakes. A light wind can displace these hotspots downwind from their source.

2.1. Dynamic of Urban Heat Islands

There are some variables that are important in terms of affecting the UHI, these factors are land cover change, urban development, lack of vegetation cover, and surface characteristics. These factors can increase the temperature of urban areas, making them warmer/hotter that the neighbouring areas.

[1] https://wp-prd.let.ethz.ch/WP0-CIPRF91243/chapter/urban-heat-islands-small-scale-climate-change/

- Urbanization and Land Cover Changes by developing more buildings and changing the land cover from vegetation to buildings (Estoque et al. (2017); Miles & Esau (2020) Cui et al. (2016))
- Surface Properties and Albedo (which is the ability of a surface to reflect the sunlight, and consequently, the heat coming from the sun) by changing the properties of the surface in urban areas for instance changing from vegetation cover or other natural landscapes to Asphalt since Asphalt has a higher albedo (Table. 1). Mohajerani et al. (2017) Suomi & Meretoja (2021).

Table. 1 Typical albedo values for various surface types (by Duhis et al., 2023)

Surface	Albedo	Surface	Albedo
Corrugated roof	0.1 - 0.15	Red/brown roof tiles	0.1 - 0.35
Coloured paint	0.15 - 0.35	Brick/stone	0.2 - 0.4
Trees	0.15 - 0.18	Oceans	0.05 - 0.1
Asphalt	0.05 - 0.2	Old snow	0.65 - 0.81
Concrete	0.25 - 0.7	White paint	0.5 - 0.9
Grass	0.25 - 0.3	Fresh snow	0.81 - 0.88
Ice	0.3 - 0.5		

- Lack of Green Spaces by removing parks, forests and other sources of vegetation (Takkanon & Chantarangul, 2019).
- Anthropogenic Heat Sources by human activities such as industrial process (Ryu and Baik, 2012).
- Urban Geometry, Building Density, and Airflow by the layout of buildings geometry such as tall buildings, which can reduce air circulation (Oke, 1988) also buy reducing air ventilation (Stewart & Oke, 2012).

2.2. Impacts of Urban Heat Islands

Urban Heat Islands (UHIs) impacts different sections including public health, energy consumption, and the environment. The UHI can occur as a result of human activities and urban infrastructure, which changes the natural energy balance, which can also leading to higher temperatures in urban areas compared to their rural surroundings.

- Public Health Impacts

1. Heat Stress and Mortality by increasing temperature in urban environments, heat related illnesses increase (Sánchez-Guevara Sánchez et al., 2017), (Arifwidodo et al., 2019).

2. Air Quality Issues by worsening air pollution since it affects and increases the rate of photochemical reactions that produce smog, which consequently leads to poor air quality. Additionally, since there are more pollutants caused by for example vehicles in cities and urban areas, UHI can increase the trapping rate of these pollutants. Solecki et al (2005), conducted a study in New Jersey, which showed that UHI contribute to increasing of air pollution.

3. Heatwaves by impacting them and consequently affecting and increasing extreme temperature periods. (Hatvani-Kovacs et al., 2016).

- Energy Demand Impacts

1. Increasing Cooling Energy Demand by leading to higher energy consumption. In Beijing, China, Xu et al (2018) found that the energy demand in 30% more in the summer in urban areas compared to rural regions. Also, Salvati et al (2017) conducted research in Barcelona and showed that cooling demand increased for around 18-28% because of UHI effects.

2. Energy Consumption by affecting economic costs and increasing them, since cooling demand increases with UHI, the subsequent costs of cooling increase as well. A research in

Bangkok, Thailand found out that with the increase in UHI, the energy bills have also increased since the need of air conditioning has increased (Arifwidodo et al., 2019).

- Environmental Impacts

1. Increasing GHG emissions, since the cooling demand increases in the areas affected by UHI, the emissions caused by energy production can increase as well. In a study by Haine & Blumberga (2023), they found out that North Africa and Europe regions that UHI can impact the increase in carbon emissions since with the increase in temperature, the energy consumption, and consequently the emissions increase, which can contribute to more climate change.

2. Urban Ecology by weakening biodiversity and ecosystems (González-Trevizo et al., 2021).

3. Water Stress: a study by Konstantinov et al., 2018, showed that in northern Fennoscandia and Arctic regions, UHI leads to permafrost thawing, weakening the soil-bearing capacity, and increasing the risk of infrastructure damage and urban flooding.

For the mitigation strategies to combat and reduce UHI effects, which have been very important for cities, there are some of them worth to be noted. The most widely studied and applied solutions include green infrastructure (GI), and urban design innovations.

- Green Infrastructure (GI) by increasing vegetation cover (Wong et al., 2021).
- Urban Design and Geometry by constructing of buildings that helps ventilation and airflow in the urban areas (Solecki et al., 2005).

3. Methodology and case study

3.1. Study Area Overview

The capital city of Sweden, Stockholm has a population of approximately 998,943 of people in the most recent data in 2023 (Statistics Sweden, 2023), Stockholm has an extensive green space with about 40% of its urban areas is green space, so it makes the city a good city compared to other capital city around the world (*Figure. 2*) (Werner, 2023). The density of population in Stockholm is high with about 5,200 people per km2, shows urban nature of the city, so it increases the demand for accommodation. This increase in population also makes to increase the density of houses, which this density of houses is about 810 houses per km2 (Statistics Sweden, 2023).

Stockholm is known for its growing fast, located in the north parts of Europe, is a good case to study UHI. This city experiences a wide range of seasonal variations, from long and cold winters to warm and short summers. All of these factors together with increase in urban areas, increase in predicted temperatures because of climate change, makes Stockholm an important case study for analysing patterns of UHI in northern latitudes. Current studies on UHI are more on temperate regions, these regions have different climate conditions compared to Stockholm. Therefore, for this reason, analysis of UHI variations in Stockholm is a good opportunity for study how cities in colder climates affected by UHI, and which mitigation strategies are more effective. Stockholm has a cold climate with the average temperature of about 7.3°C (Climate-Data.org, n.d[2]) and the average precipitation of this city is about 619 mm/year (Climate-Data.org, n.d).

[2] https://en.climate-data.org/

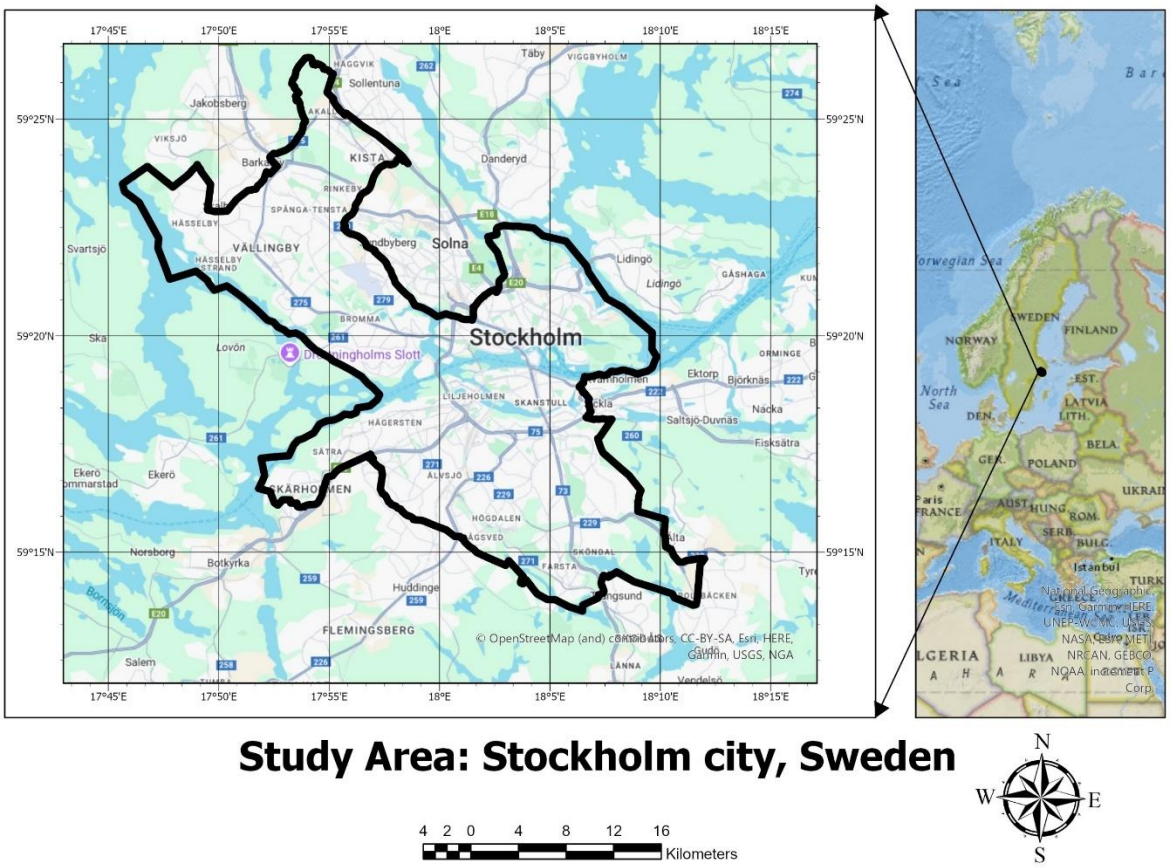

Figure. 2 Stockholm, Sweden

3.2. Datasets

3.2.1. Temperature Maps

Temperature maps used in this analysis are created with the data collected from Netatmo weather stations, which are devices that measure and monitor various environmental conditions. These stations are a part of a dense network, that include a big, interconnected users contributing to a global database of weather information and are installed across different regions by the individual people. These stations data can be considered as local weather data, at a much smaller scale than national meteorological stations, these stations provide precise weather data specifically for an exact location. From this data, temperature maps with high resolutions (30-meter) are created. These maps help to analyse temperature variations in

different regions of Stockholm. These maps are used to create UHI maps, which help to show monthly variations of UHI for 2014-2023.

3.2.2. Vegetation and Urban Indices

To extract vegetation and built-up surface information, this study uses three well-known indices derived from remote sensing data: NDVI (Normalized Difference Vegetation Index), NDBI (Normalized Difference Built-up Index), and LSA (Land Surface Albedo). These indices are calculated using satellite imagery from the Landsat 8 program, which is a joint NASA/USGS (United States Geological Survey) initiative, launched in 2013 and it provides the longest continuous, space-based record of Earth's land surface. All of these indices were extracted using Google Earth Engine (GEE), which offers the necessary spectral bands at 30-meter resolution.

- *Normalized Difference Vegetation Index (NDVI)*

NDVI is used to quantify vegetation cover within the study area. It is calculated using the following Eq. (Rouse et al., 1974):

$$NDVI = \frac{(NIR-RED)}{(NIR+RED)} \quad (1)$$

where, *NIR* is reflectance of light in the near-infrared band and *RED* is reflectance of light in the red band. NDVI values range from -1 to +1, where higher values indicate dense and healthier vegetation, while values close to 0 or negative indicate non-vegetated surfaces like water, bare soil, or urban areas (*Figure. 3 and 4*). When a vegetation is under stress or there is no vegetation at all, they absorb less red light and reflects more of the red light, but reflects less of near infrared light, on the other hand a healthy vegetation, absorbs most of the red light but reflect the near infrared light strongly. By comparing the amount of red and near-infrared light

reflected, NDVI can help to see the difference between vegetation, water, bare soil, and other surfaces.

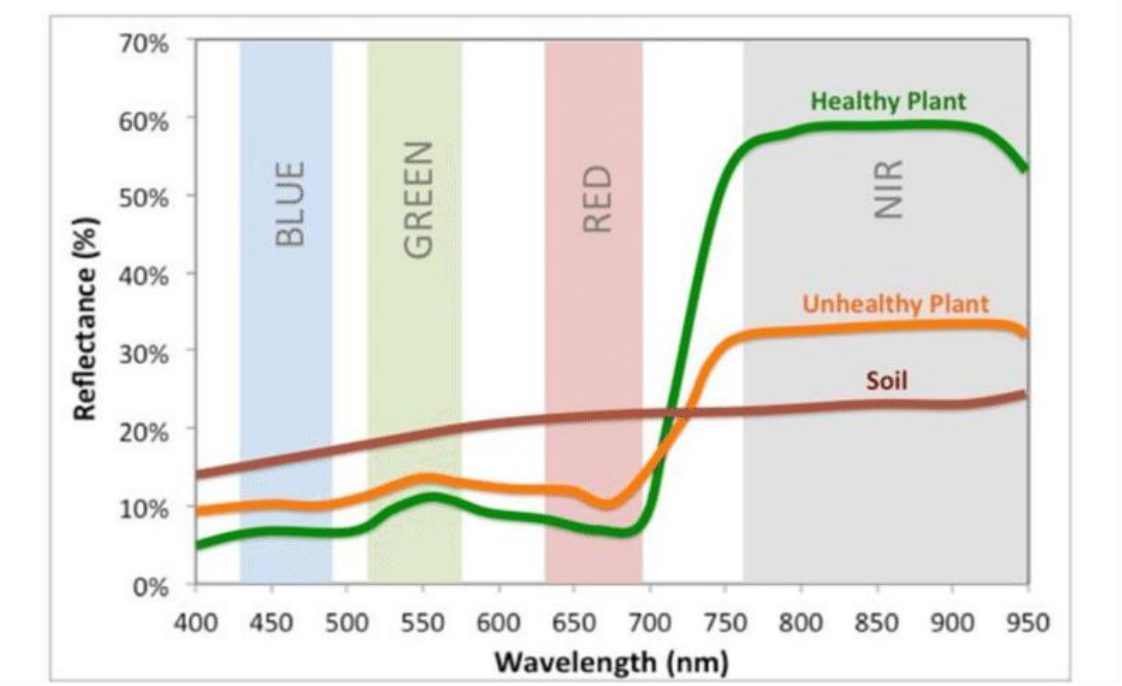

Figure. 3 Healthy vegetation has a higher reflectance within the nIR region (by Lum et al., 2016)

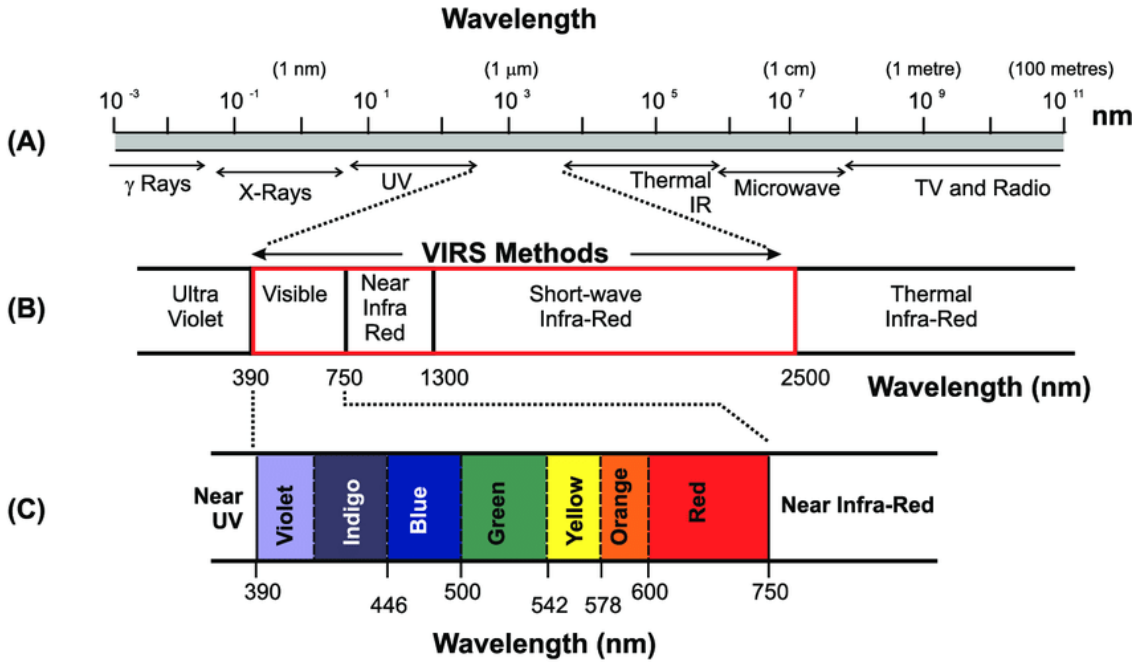

Figure. 4 The electromagnetic spectrum (By Kerr et al., 2011)

- *Normalized Difference Built-up Index (NDBI)*

NDBI is a measure of urbanization and built-up areas. It is computed using the following Eq. (Zha et al., 2003):

$$NDBI = \frac{(SWIR-NIR)}{(SWIR+NIR)} \quad (2)$$

where, *SWIR* is reflectance in the shortwave infrared band and *NIR* reflectance in the near-infrared band. Positive NDBI values indicate built-up areas with high urban density, while negative values generally correspond to vegetated or water-covered regions.

- *Land Surface Albedo (LSA)*

Land Surface Albedo (LSA) basically shows how much sunlight is reflected by the Earth's surface. It's usually defined as the ratio between reflected solar radiation and the incoming radiation:

LSA=Incoming Light/Reflected Light

This means surfaces like snow or bright roofs reflect a lot (so their albedo is close to 1), while dark surfaces like asphalt absorb most of the energy, giving them an albedo closer to 0.

Now, to estimate LSA more accurately from satellite data, we don't just use a simple ratio, we apply a weighted formula based on the spectral bands of the sensor (Liang, 2001):

$$LSA = \sum(R_i \,.\, \omega_i) \quad (3)$$

where, R_i is reflectance in each band and ω_i is weighting factor for each band, based on its contribution to the total albedo. The specific weights and bands depend on the sensor used. High albedo values (close to 1) represent highly reflective surfaces like snow or light-colored materials, while low albedo values (close to 0) indicate heat-absorbing surfaces such as asphalt or dark roofs.

3.2.3. Wind Speed

- *Wind speed data acquisition*

Wind speed data were obtained from ERA5 reanalysis. ERA5 is a global climate dataset developed by the European Centre for Medium-Range Weather Forecasts (ECMWF) under the Copernicus Climate Change Service. This program is a part of the European Earth Observation programme. ERA5 provides a variety of high-resolution data for meteorological variables including wind variables, like u_{10} and v_{10}, which were used for wind speed analysis. The two variables correspond to eastward and northward wind speed at 10 m above the ground and offer a directional breakdown of wind patterns (Dupuy et al., 2023).

To derive wind speed, the following Eq. is applied (Li et al., 2025):

$$WS = \sqrt{(u_{10})^2 + (v_{10})^2} \quad (4)$$

This equation allows to convert the vector components into a single scalar value, representing wind speed at each grid point. This step is widely used in meteorological studies to obtain wind speed estimates from reanalysis data (Alizadeh et al., 2019).

- *Geostatistical downscaling approach*

High-resolution wind speed data were created using geostatistical downscaling. This method ensures the preservation of small-scale details in the data; therefore, resulting in more accurate and better representation of local scale variables like wind speed (Tang and Bassill, 2018).

Since the ERA5 wind data are coarse, they were downscaled using land cover/land use data. To downscale these data, LULC data were used to calculate surface roughness, since we need the values of surface roughness to perform geostatistical downscaling. Surface roughness in consider as the ability of a surface to resist airflow and consequently affect wind speed. Each LULC type has a unique roughness value (Meier et al., 2022). These values were used to assign

weights in each ERA5 grid cell, allowing the coarse wind speed to be adjusted (for instance there are areas with high development or vegetation, which lead to lower wind speed and there are open areas, which leads to increase wind speed) (Marsh et al., 2023). This method helps to produce wind speed dataset that better show local variations (Fu et al., 2024).

3.2.4. Reference Temperature

The intensity of UHI can only be calculated using non-urban reference points, which were supplied as rural temperatures in this research. Monthly and seasonal reference temperatures were estimated based on data from a Netatmo weather station with negligible human activity and development outside the study area. The conditions at the reference stations provide reference points to quantify UHI and analyse its trends.

Table 2. Data Sources and Specifications

Dataset	Source	Spatial Resolution	Temporal Resolution
Temperature	Netatmo	~30 m	monthly
Wind Components (u10, v10)	ERA5 (ECMWF)	~30 km	monthly
NDVI, NDBI, LSA	Landsat 8	30 m (spatial)	monthly
Reference Temperature	Netatmo (Rural station)	Station-specific	monthly

3.2.5. Local Climate Zone (LCZ)

The studies of UHI, are mainly discussed with regards to local field sites, which have different physical and climatological characteristics. These sites are referred to as urban and rural areas, which can cause some uncertainties for the impact of land cover in the respective sites. To address this issue, the “local climate zone” (LCZ) classification system has been developed. The LCZ system introduces 17 different zones, which represent at a local scale. Each type has a unique combination of different characteristics including surface structure, cover, and human

activity. This system provides a standard framework for reporting and comparing field sites and their representative temperature records. Although the LCZ system at first was introduced for urban heat island studies, it can also be used for city planning, investigation of landscape ecology, and global climate change studies (Stewart & Oke, 2012) (*Figure. 5*).

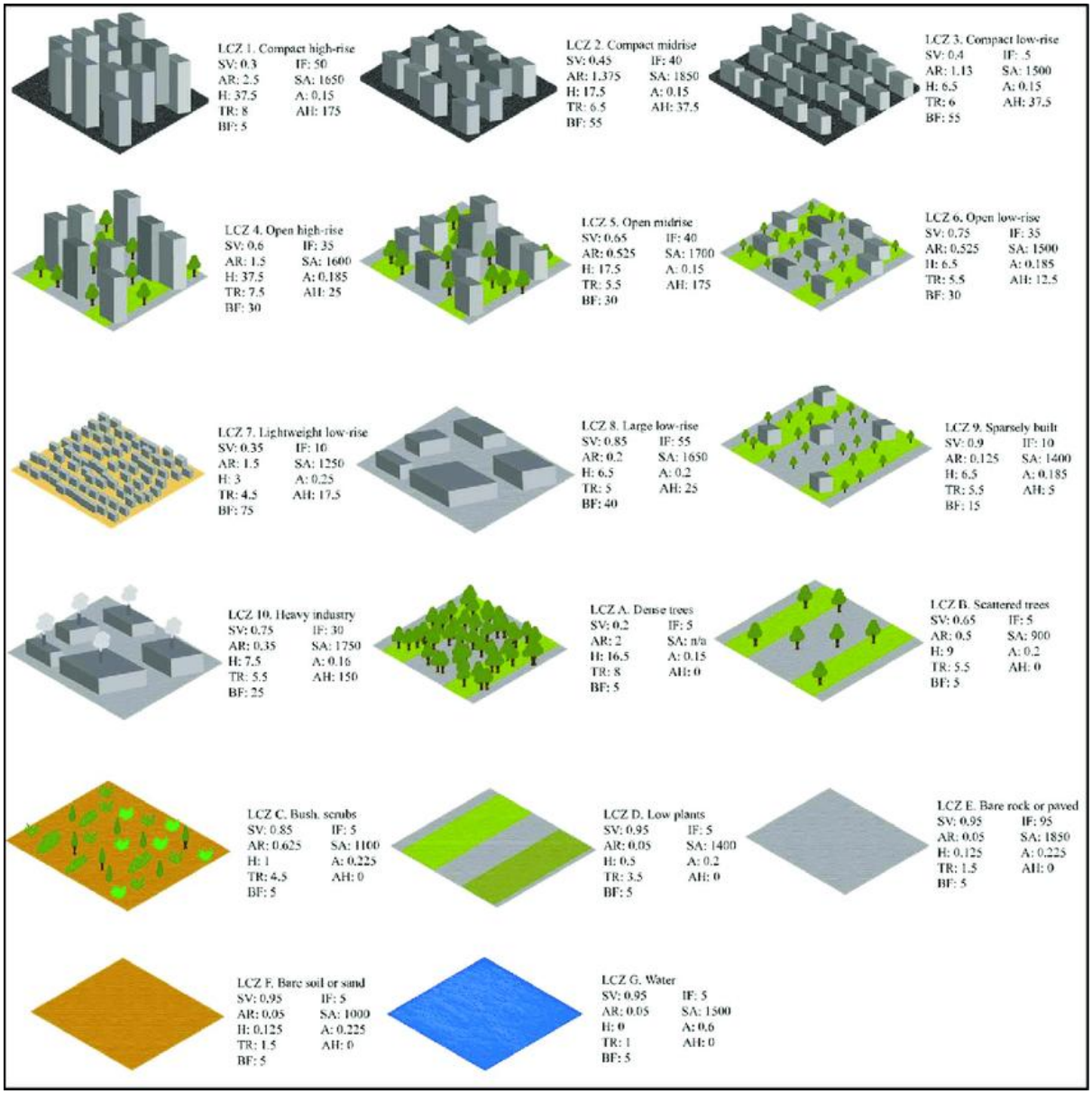

Figure. 5 Local Climate Zone Classes

3.3. UHI Intensity Calculation and Classification

All raster layers are standardized to a spatial resolution of 30 m for ensure compatibility and reduce distortion. Furthermore, identical resolution improves processing efficiency and reduces computational burden, as well as ensuring the accurate representation of spatial features. UHI, representing the temperature difference between urban areas and the rural reference points, is calculated according to Voogt and Oke (2003) as follows:

$$UHI\ Intensity = T_{urban} - T_{rural} \quad (5)$$

where, T_{urban} is air temperature of the urban area and T_{rural} is air temperature of the corresponding rural reference area.

After calculating UHI intensity using the above formula, we classify the results into 6 different classes to make the results better understandable and comparable. These classes are shown in the *Table 3*:

Table 3. UHI intensity classification

Classes	UHI
Very Low	UHI <= 1
Low	1 < UHI <= 2
Moderate	2 < UHI <= 4
High	4 < UHI <= 6
Very High	6 < UHI <= 8
Extreme	UHI > 8

Previous research (e.g., Oke, 1982) was adopted as the basis for UHI intensity categorization, but adjustments were made to tailor the categories for Stockholm. Typical summer UHI

intensities in Stockholm range between 1°C and 4°C but might exceed these values during extreme events such as the 2018 heatwave, when UHI intensity exceeded 6°C (SMHI, 2019[3]).

These thresholds are not official policy standards but have been adapted to reflect Stockholm's specific climate and urban layout. They offer a locally relevant way to identify areas at high risk from heat and to help focus mitigation and adaptation efforts, especially as temperatures rise and heatwaves become more frequent.

3.4. Creation of Local Climate Zone (LCZ) Map

- *Local Climate Zone (LCZ)*

The LCZ base map was generated based on land use maps through reclassifying land use categories into LCZ classes in ArcGIS according to standard definitions, similar to previous research such as Perera & Emmanuel (2018) and Danylo et al. (2020). The workflow by Quan et al (2018) was adopted in this study, wherein each land use is initially considered to be an LCZ and is subsequently refined using parameter overlays.

- *LCZ classification*

LCZ map was created with the help of a land use map of the area, which was a base map, and after that was better refined to have the LCZ map using several calculated parameters. These include:

1. Building Surface Fraction (BSF): Proportion of building area to total area.

   The building surface fraction was calculated using the building footprint data. These data are in vector format, so for a better analysis they are converted to raster format. The pixels, which have buildings in them are assigned as 1 but the other pixels without buildings were assigned 0. Then, BSF was calculated dividing the number of building

[3] https://www.smhi.se/en

pixels by the total number of pixels for each cell. These approach considers a uniform coverage, so it may not show a good representation of the areas with mixed land cover

2. Average Building Height (BH): Mean building height in the study area.

   To calculate BH, first, a Digital Surface Model (DSM) was used, and then the average height for each cell was directly extracted and calculated.

3. Road Density: Total road length per grid cell.

   At first stage the road width is calculated. Since the road density file was in the vector format, this format was then converted to raster for easier analysis to calculate the roads in each cell. The accuracy of this approach depends on the datasets available for the analysis.

4. Vegetation Coverage Ratio (VCR): Proportion of vegetation-covered area to total area.

   It was calculated from NDVI rasters created using satellite images. The proportion of vegetated pixels within a cell gives the VCR. Although this method works well for identifying green areas, it can be affected by the time of year the satellite image was taken, since NDVI values vary with the season and weather conditions.

5. Impervious Surface Fraction (ISF): Proportion of impervious surfaces to total area.

   This was calculated using land cover rasters that classify artificial surfaces. The number of impervious pixels was divided by the total number of pixels in each cell to get the ISF.

6. Sky View Factor (SVF): Representing the openness of the sky at ground level.

Calculated using the weighted height raster to approximate visible sky, following approaches outlined in Ren et al. (2020).

Each of these parameters plays a role in distinguishing LCZ types, from dense urban environments to vegetative and open spaces (Zhou et al., 2021; Qiu et al., 2018). *Table 4* shows the different LCZ classes in the case study area.

Table. 4 Local Climate Zone (LCZ) classification in the study area

LCZ Class	Description
LCZ A	Dense trees: Forests with high, continuous canopy cover.
LCZ C	Bushes: Shrubs or bushes with minimal canopy height.
LCZ D	Low plants: Grasslands, meadows, or agricultural fields.
LCZ E	Bare rock or paved: Hard surfaces with no vegetation.
LCZ F	Bare soil or sand: Loose, exposed soils or sandy areas.
LCZ G	Water: Rivers, lakes, or other permanent water bodies.
LCZ 2	Compact mid-rise: Moderately dense areas with mid-rise buildings.
LCZ 3	Compact low-rise: Dense areas with low-rise buildings.
LCZ 5	Open mid-rise: Mid-rise buildings with open space.
LCZ 6	Open low-rise: Low-rise buildings with open space.

LCZ 8	Large low-rise: Large low-rise structures
LCZ 9	Sparsely built: Scattered small buildings with open land.
LCZ 10	Heavy industry: Industrial areas with low and midrise structures.

- *Classification process*

The classification process started by developing an LCZ base map on the existing land cover and land use data, which was reclassified into LCZ types based on the findings of Perera and Emmanuel (2018) and Danylo et al. (2020). Final LCZ types were connected to the different land use classes to create the first baseline, which would be modified later on. To accomplish this, attributes correlating to the crucial urban morphology determinants were calculated, specifically Building Surface Fraction (BSF), Average Building Height (BH), Road Density (RD), Vegetation Coverage Ratio (VCR), Impervious Surface Fraction (ISF), and Sky View Factor (SVF). These attributes were created from constant raster layers based on spatial analysis tools in ArcGIS, such as the Raster Calculator and 30m spatial resolution. Then, the LCZ base map was modified based on these factors of consideration through raster overlay, which follows what other research studies had accomplished, such as in Quan et al. (2018), where findings emphasized that spatial variability across a type of urban form and characteristics could enable more accurate final classifications. The resulting raster had values ranging between 1.45253 and 16.4526, which were assessed and reclassified based on threshold values established from the literature review, while accuracy was confirmed through visual validation with the satellite imagery and land cover data. Therefore, the resulting map was an effective representation of the characteristics of spatial variability between urban and natural

areas of the study location, which provided further confidence in the classification process. (*Figure. 6*).

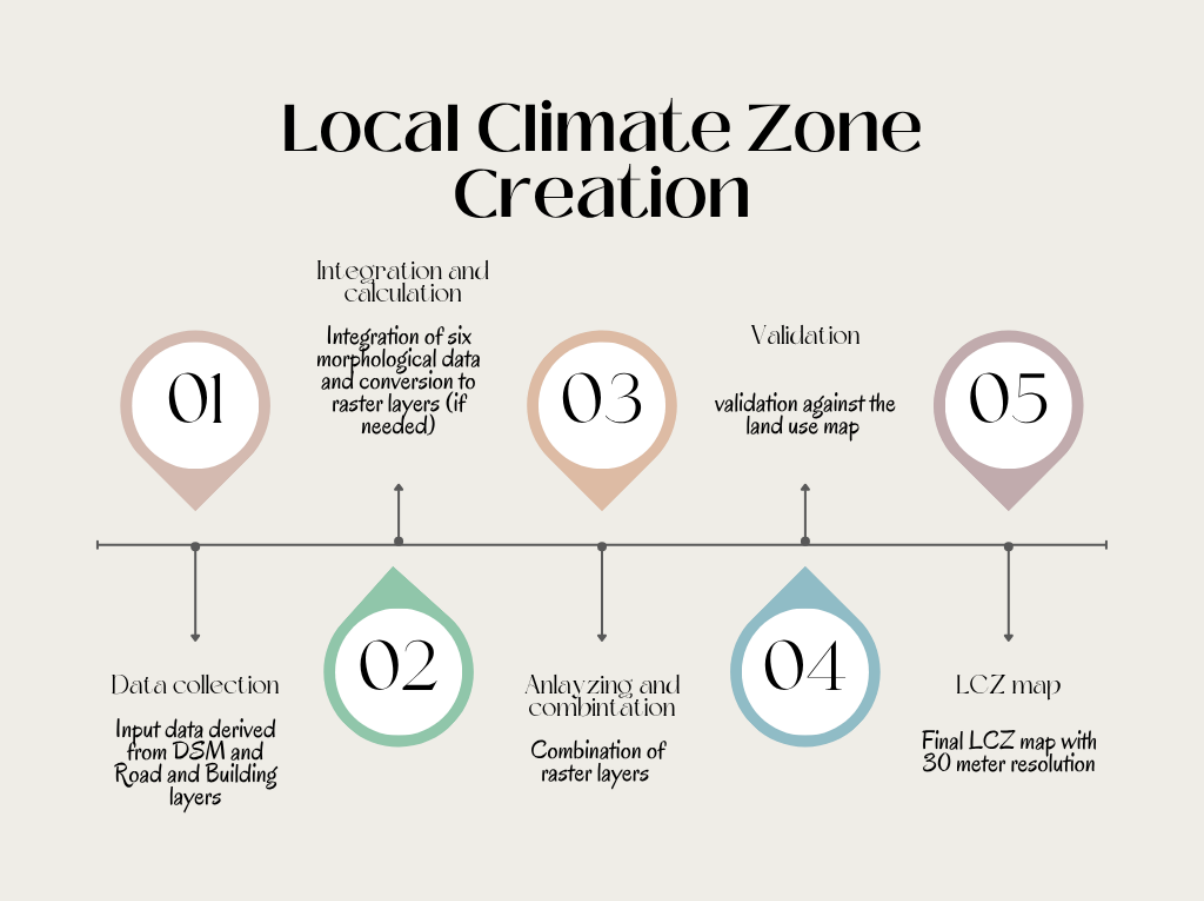

Figure. 6 Local Climate Zone Map Creation Process

3.5. Machine Learning Models

Linear Regression

Linear regression is a simple yet capable method of modelling a relationship between a depended variable Y (here, UHI) and independent variables X_i (here, indices). The general equation for a linear model is represented as (Maulud & Abdulazeez, 2020):

$$Y = \beta_0 + \sum_{i=1}^{n} \beta_i X_i + \epsilon \quad (6)$$

Where:

- Y is dependent variable, $X_i$is independent variable *i*., β_i is coefficient for the independent variable *I*, and ϵ is error term.

Support Vector Regression (SVR)

SVR is a robust regression technique designed for high-dimensional datasets. Unlike linear regression, it uses kernel functions to map data into higher dimensions, allowing it to model non-linear relationships. Its objective is to find a function $f(x)$ that approximates the true target y, minimizing prediction errors within an ϵ insensitive region (Vapnik, 1995):

$$min\left(\frac{1}{2}\|\omega\|^2 + C\sum_{i=1}^{n}\max\left(0, |y_i - f(x_i)| - \epsilon\right)\right) \quad (7)$$

Where:

- ω: Weight vector.
- C: Regularization parameter.
- ϵ: Margin of tolerance.

SVR is particularly effective in urban climate studies due to its ability to handle sparse, noisy datasets while maintaining high generalization accuracy (Awad et al., 2015).

Decision Tree Regressor

Decision tree regression operates by deconstructing a complex decision into simpler component parts, making it easier to understand (Breiman, 2017). In the context of geographical and spatial analysis, data features represent the predictors and the target variables is considered to be continuous. Decision tree regression represents an efficient technique for analysing non-linear relationships between spectral bands and mixed pixel class proportions. Another advantage of this method is the selection of the most informative features while performing feature selection and classification, which further improves efficiency by

eliminating less informative features. The dataset is progressively divided into smaller groups to minimize variance, measured using Mean Squared Error (MSE):

$$MSE = \frac{1}{N}\sum_{i=1}^{N}(y_i - \hat{y}_i)^2 \quad (8)$$

Where N is Number of samples.

K-Neighbors Regressor

This algorithm predicts by averaging the values of the k-nearest neighbors. It is simple and interpretable but struggles with high-dimensional data due to the "curse of dimensionality" (Altman, 1992).

$$\hat{y} = \frac{1}{k}\sum_{i=1}^{k} y_i \quad (9)$$

Where:

- y_i: Values of the nearest neighbors.

Random Forest

Random Forest (RF) is a machine learning method that uses multiple decision trees created from random samples of data. It selects a subset of predictors at each split, reducing tree correlation and improving model accuracy (Breiman, 2001). Important parameters include the number of predictors per split and minimum node size. It also uses proximity matrices to identify outliers by measuring how far observations deviate from others (Izenman, 2008):

$$\hat{y} = \frac{1}{M}\sum_{j=1}^{M} f_i(X) \quad (10)$$

Where:

- $f_i(X)$: Prediction from tree j.
- M: Number of trees.

Extra Trees Regressor

This method constructs a decision tree, but using randomized splits. Although this method is faster than Random Forest, the results are more difficult to interpret (Breiman, 2017).

XGBoost

XGBoost (Extreme Gradient Boosting) is a powerful ensemble algorithm that optimizes decision tree performance through gradient boosting. It uses regularization techniques to prevent overfitting and is known for its high accuracy and efficiency in competitive modeling tasks. XGBoost is particularly effective in managing missing data and capturing non-linear relationships (González et al., 2020; Chen & Guestrin, 2016):

$$L = \sum_{i=1}^{n} l(y_i, \hat{y}_i) + \lambda \|\omega\|^2 \quad (11)$$

Where:

- $l(y_i, \hat{y}_i)$: Loss function.
- λ: Regularization parameter.

3.6. Model Evaluation Metrics

To assess the performance of the machine learning models used for predicting UHI intensity, several standard evaluation metrics were employed. These metrics evaluate how well the predicted UHI values match the observed or ground-truth values, allowing for objective comparison of model accuracy and reliability.

Models are evaluated using the following metrics:

Root Mean Squared Error (RMSE): Measures prediction error, emphasizing larger deviations:

$$\text{RMSE} = \sqrt{\frac{1}{N}} \sum_{i=1}^{N} (y_i - \hat{y}_i)^2 \quad (12)$$

This metric highlights larger errors by squaring the deviations, making it particularly sensitive to outliers (Chai & Draxler, 2014).

Coefficient of Determination (R^2): Quantifies the proportion of variance explained by the model:

$$R^2 = 1 - \frac{\sum_{i=1}^{N}(y_i - \hat{y}_i)^2}{\sum_{i=1}^{N}(y_i - \hat{y})^2} \quad (13)$$

This metric measures the goodness-of-fit of the model, with values closer to 1 indicating higher predictive power (Nagelkerke, 1991).

Mean Absolute Error (MAE): Measures the average magnitude of prediction errors, offering a straightforward interpretation:

$$MAE = \frac{1}{N}\sum_{i=1}^{N}|y_i - \hat{y}_i| \quad (14)$$

Unlike RMSE, MAE treats all errors equally without emphasizing larger deviations (Willmott & Matsuura, 2005).

These metrics collectively assess both predictive accuracy and model efficiency, enabling robust evaluation and comparison.

3.7. Climate Change Projections Methodology

The dataset includes a number of downscaled projections based on General Circulation Models (GCMs) developed for the CMIP6 project. Due to their global nature, GCMs utilize a coarse resolution (~100 km), while the data offered by NASA NEX-GDDP-CMIP6 are available at a smaller resolution (~25 km). The period from 1984 to 2000 comprised the historical portion of the dataset; projections were made for until 2100 using a range of greenhouse gas emission scenarios.

We used climate model results and the data from Netatmo in Stockholm in this thesis and the station data give us a good baseline for seasonal temperatures from 2014 to 2023.

The methodology involves:

1. Extracting seasonal mean temperatures (summer and winter) from each selected climate model for both historical (1984–2014) and future periods (2030–2039).
2. Calculating the difference (anomaly) between future and historical seasonal means for each station location.
3. Adding these anomalies to the observed recent seasonal means from the Netatmo stations to generate station-specific seasonal temperature projections under each emission scenario.
4. Organizing the projected seasonal temperatures into an Excel workbook, structured by year, station, season, and scenario, to enable detailed temporal and spatial analysis.

3.7.1. Climate Models Used (ACCESS-CM2 and CESM2)

For the CC projection, we used two General Circulation Models (GCMs) from the NASA NEX-GDDP-CMIP6 dataset, the first one is “ACCESS-CM2” and the second one is “CESM2”.

3.7.2. Emission Scenarios (SSP1-2.6 and SSP5-8.5)

For projection of climate change, we consider two different SSPs (Shared Socioeconomic Pathways) scenarios, SSP1-2.6, which is the best-case scenario, and SSP5-8.5, which is the worst-case scenario when considering the greenhouse gas emission.

SSP1-2.6 represents conditions where nations across the world minimize emissions, use clean energy, and adhere to strict climate regulations, leading to minimal temperature changes. On the other hand, SSP5-8.5 presents the conditions where the widespread use of fossil fuels

persists, climate action is general disregarded, and energy use keeps pace with rapid economic growth, leading to significant rise in global temperatures.

The resulting temperatures from both scenarios are then compared to the historical reference temperature from 1984-2014 and when we have significant differences we considered them as temperature anomalies. These temperature changes are added to the real temperatures observed from Netatmo weather stations in Stockholm for 2014 to 2023. This method is called delta change method. It works by taking the current observed temperature and adding the projected change. This way, we get the future temperature estimates for each station under both scenarios.

We use delta change method because it is simple and strong. It helps combine detailed local data with big scale climate model results. This way, the study can give a good idea how UHI might change in Stockholm in the next years.

4. Results

4.1. Local Climate Zone (LCZ) Map Analysis

After completing the initial UHI analysis, a LCZ map was created to enhance the classification of the study area and improve the understanding of the relationship between urban morphology and UHI intensity (*Figure. 7*). The map shows that there are 13 different classes in the study area, which are 4 classes less than the original classification. The classes, which are not in the area are LCZ B, LCZ 1, LCZ 4, and LCZ 7, which represents scattered trees, dense urban areas with tall buildings, tall buildings with significant open space, and lightweight low-rise, respectively. LCZ helps us to have a more in depth understanding of how different urban characteristics can affect the UHI.

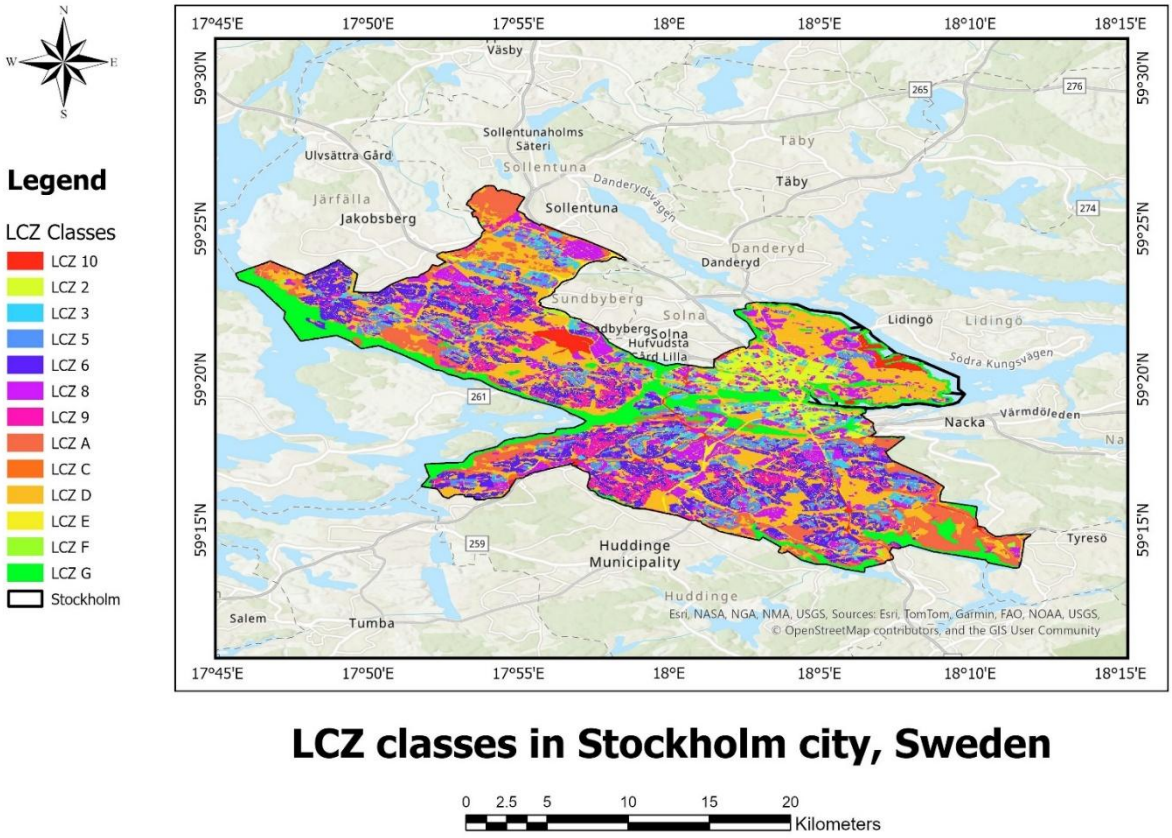

Figure. 7 Local Climate Zone (LCZ) map of Stockholm city, Sweden

4.2. UHI Mapping Results

The generated maps for each season highlight areas experiencing varying levels of UHI intensity. The maps were classified based on the table below:

Table. 5 Classification of the UHI threshold

Classes	Threshold (°C)
Very Low	UHI <= 1
Low	1 < UHI <= 2
Moderate	2 < UHI <= 4
High	4 < UHI <= 6
Very High	6 < UHI <= 8
Extreme	UHI > 8

In the winter of 2014, January to February experienced the most UHI amongst the other months. In this month the UHI was mostly moderate and high, especially in areas that did not experience more UHI. For instance, in the northwest parts of Stockholm in other months, there were only low values of UHI, however, in January to February these areas faced moderate and high UHI. On the other hand, in the summer, the UHI mostly were low to moderate and in small parts high and very high. In the three months of summer, the UHI had similar shape (*Figure. 8*).

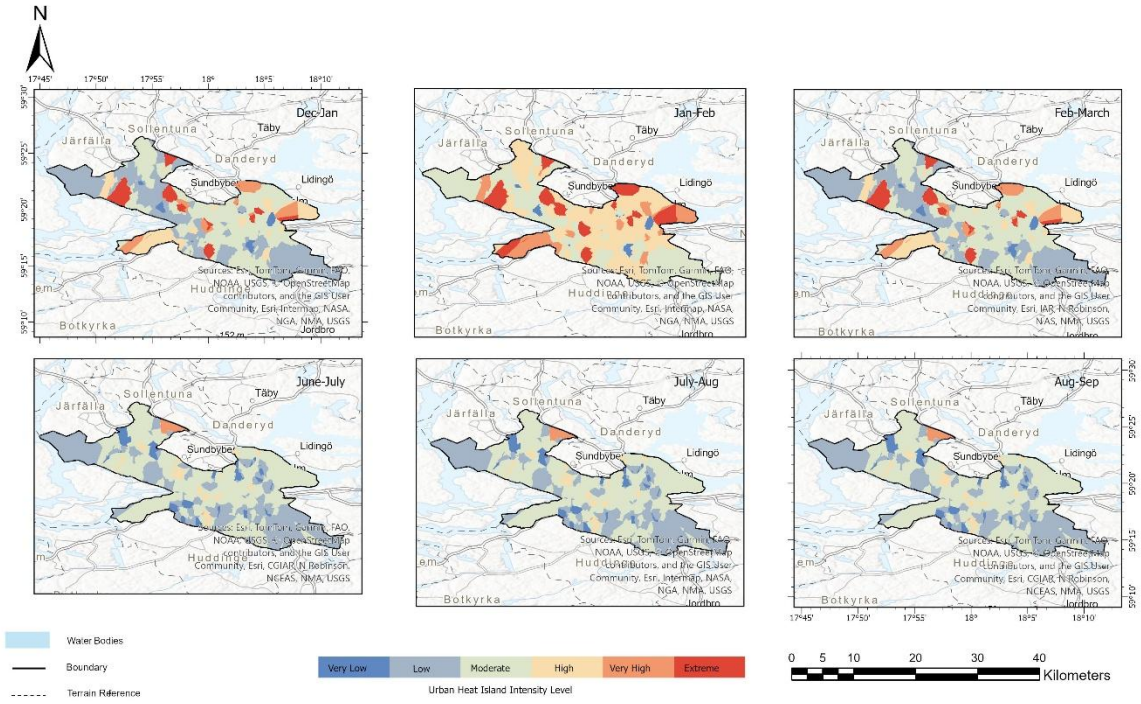

Figure. 8 UHI Intensity Map for 2014

In 2015, the UHI patterns were different between the winter and summer seasons. From December to March, the Urban Heat Island was mostly moderate to high, and in some parts even very high and extreme. For example, in Dec-Jan the central and eastern areas like around Sundbyberg (in the central parts of the cast study) had many very high and extreme spots of UHI. These places maybe did not face such strong UHI in the other months. In Feb-March, also many areas showed higher UHI compared to Jan-Feb, especially again in central Stockholm.

In summer months like June-July, the UHI was mostly low and very low. Large areas were blue and light blue, which means not so much UHI during that time. July-Aug had similar pattern. There were some small parts with moderate UHI (yellow), but mostly the map shows cool or less heated areas. However, in Aug-Sep there were higher UHI values in the case study.

In general, winter again had stronger UHI than summer in 2015. Also, the shape and pattern of UHI in summer was similar across the first two months, and in winter the highest values appeared more in Dec-Jan and Feb-March (*Figure. 9*).

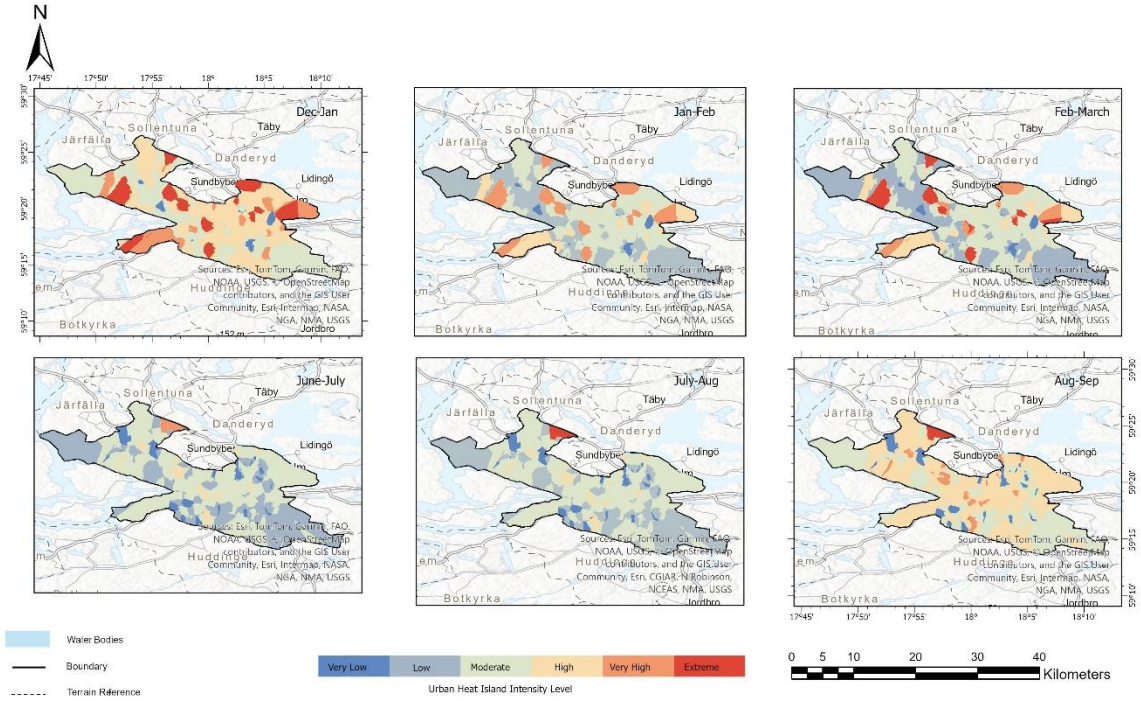

Figure. 9 UHI Intensity Map for 2015

In 2016, the UHI in the winter months showed a clear pattern where Jan-Feb had the strongest UHI compared to the other months. In this period, many areas in central Stockholm, especially around Sundbyberg and the inner districts, experienced high and very high UHI values. Even places that usually had low UHI in other months showed moderate to high values in Jan-Feb. In the months of Dec-Jan, we had moderate class as the main class spread in different parts of the case study but there are some parts with high class of UHI in the west parts of the area. In Jan-Feb, we have areas with extreme class showing a big temperature difference between these areas and rural areas. But in Feb-Mar, these differences are less and the UHI is very similar to Dec-Jan month.

In the summer of 2016, the UHI was mostly low to moderate. In June-July, most areas showed moderate to high UHI. July-August had lower UHI than June-July, with larger parts of the city showing light blue colors, meaning less UHI. In Aug-Sept, there was a very slight increase again, with some moderate UHI values appearing in central areas. But in general, the summer UHI was weaker than winter, and the shape of the UHI zones in summer was more stable across the months (*Figure. 10*).

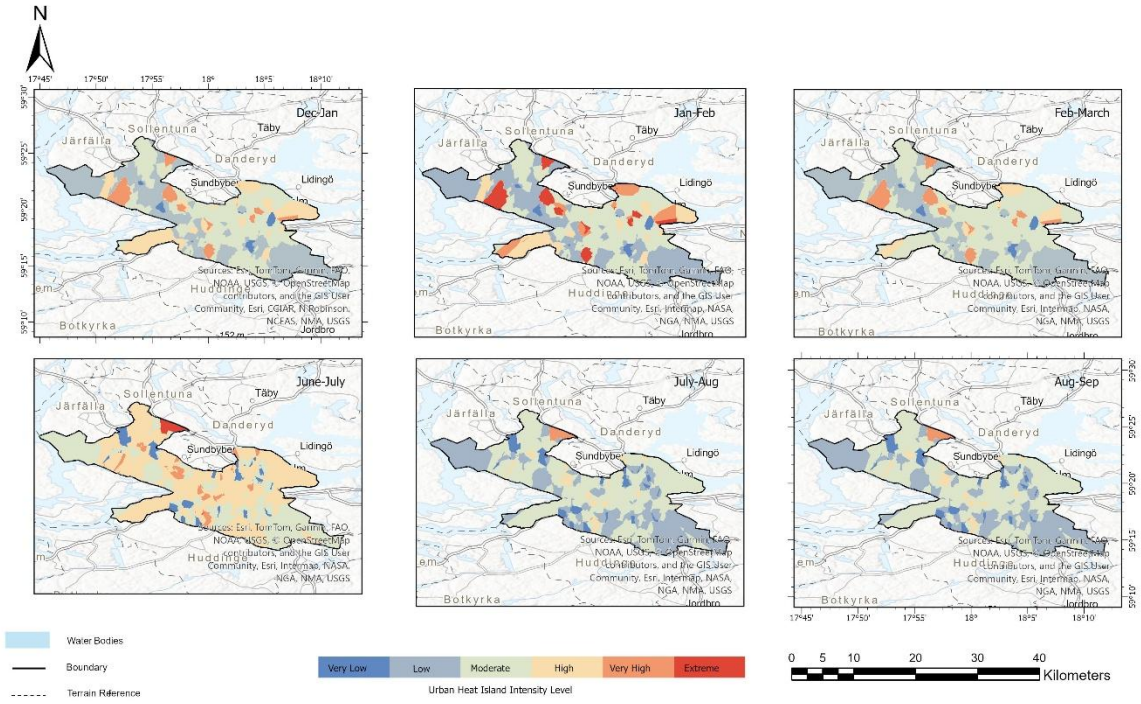

Figure. 10 UHI Intensity Map for 2016

In 2017, the UHI in winter was again strong, Dec-Jan was the month with the highest UHI. In that period, many areas in central and northeast Stockholm had very high and even extreme UHI values. These areas had much stronger UHI than in Jan-Feb or Feb-March. In Jan-Feb, the UHI was mostly moderate to high, especially in areas like south part of Stockhom, where very high UHI spots were visible. In Feb-March, some parts still had high UHI, but the intensity slightly decreased compared to Dec-Jan and Jan-Feb. Still, central Stockholm remained warmer than the surroundings.

In the summer of 2017, the UHI was quite low. In June-July, many areas were blue and light blue, meaning very low or low UHI. The central zones had less UHI than usual. In July-Aug, the UHI stayed very low, and only a few small areas had moderate values. This was one of the coolest periods in the summer maps. In Aug-Sept, UHI increased a little again, especially in the central parts where some yellow zones appeared. But overall, just like in 2016, the winter UHI was much stronger than the summer, and the UHI shape was similar across the three summer months (*Figure. 11*).

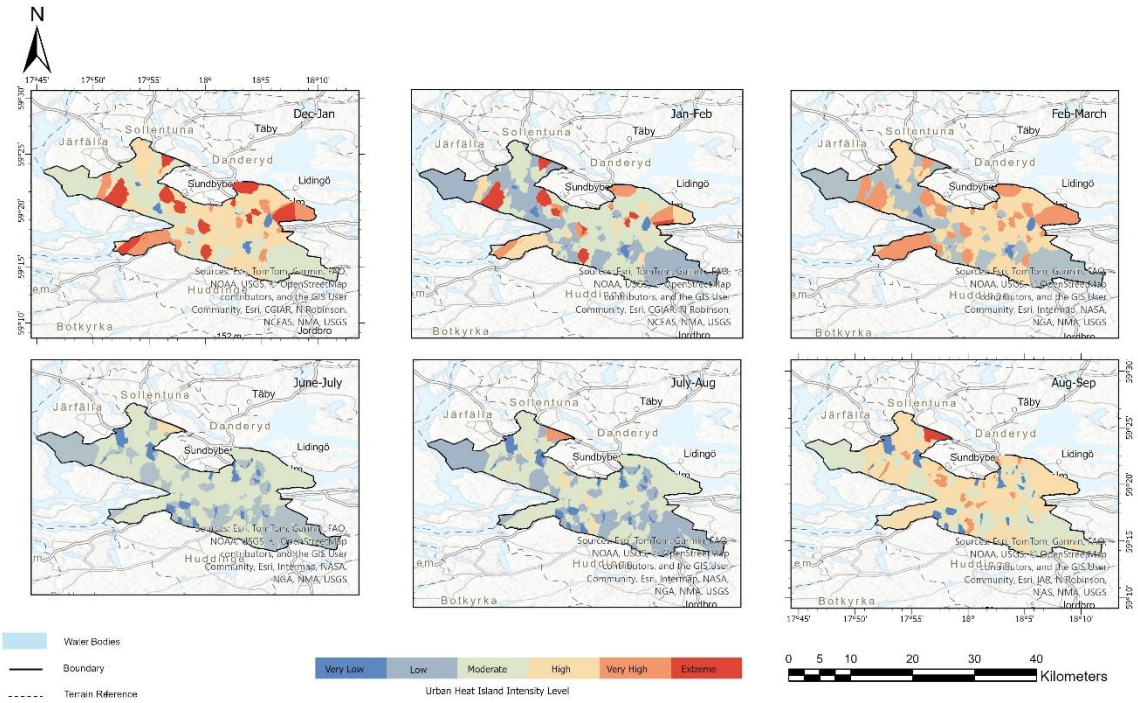

Figure. 11 UHI Intensity Map for 2017

In 2018, the UHI patterns in the winter season showed noticeable differences between the months. Jan-Feb experienced the lowest UHI compared to the other winter months, with most parts of the map showing low and very low UHI intensity. The areas were mostly blue, meaning they were not much affected by UHI during this period. But in Feb-March, the intensity of UHI increased clearly. The most noticeable part was in the northern area of Stockholm, especially around Kista, where UHI values became high and even very high. These zones that are usually

more built-up and urbanized had strong UHI effect during this month. Dec-Jan was more in between, with the UHI mostly in the moderate level. There were no large areas with very low or very high UHI and it stayed around average values. In the summer season, the patterns changed again. June-July had the lowest UHI of the three months, and large parts of the map were light blue, showing cool temperatures and weak UHI. In July-Aug, the UHI increased, especially in the central parts of the case study, where yellow and orange areas appeared, meaning high and very high UHI. This was the hottest month in the summer of 2018. Aug-Sept came next with lower intensity than July-Aug, but still more than June-July. So, the summer of 2018 had a gradual rise and fall, with the strongest UHI in the middle month (*Figure. 12*).

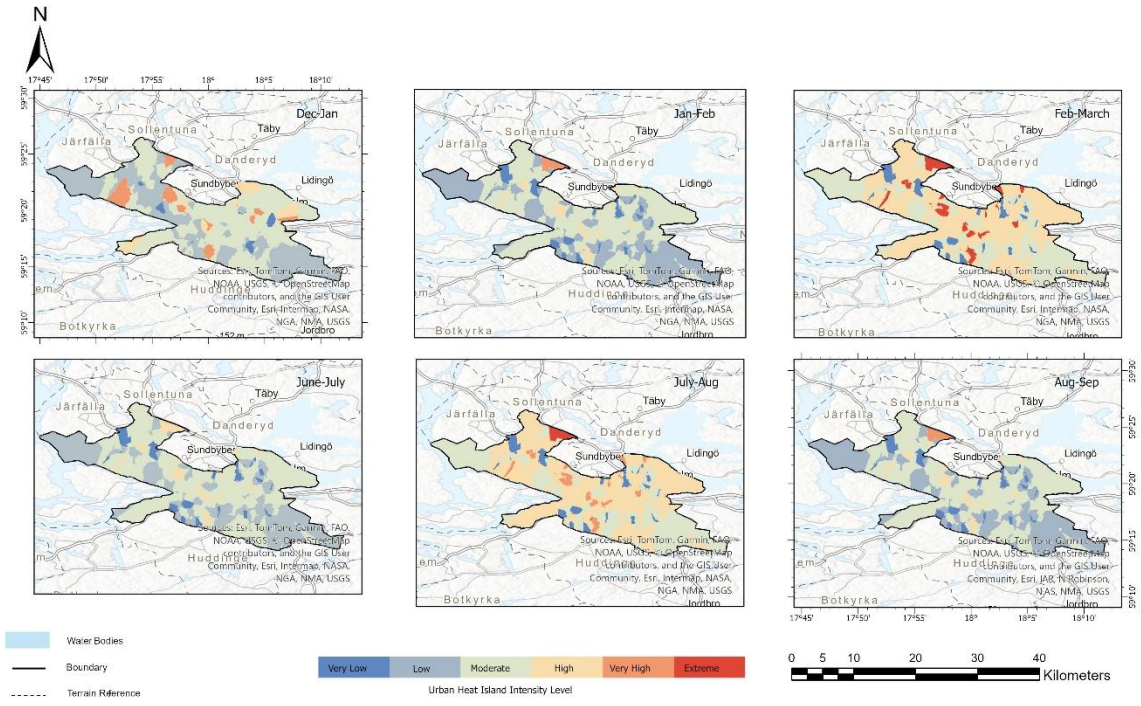

Figure. 12 UHI Intensity Map for 2018

In 2019, the UHI intensity in the winter was stronger than in 2018. Jan-Feb had one of the highest UHI intensities, with only a few small spots showing low UHI. Most of Stockholm was covered in moderate to extreme UHI values, especially in places that are more urbanized. This month really stood out in terms of heat accumulation. Dec-Jan and Feb-March also showed

strong UHI, and the pattern between them was quite similar. In both maps, places like Kista and other dense zones had higher UHI. These are the areas where population and buildings are more concentrated, so they usually have stronger UHI during colder seasons. The maps didn't change a lot in shape between these two months, but the intensity was quite consistent and strong. In the summer of 2019, the pattern was more stable. June-July and Aug-Sept both had similar UHI distribution. Most parts of the map were in low to moderate levels, with not many areas having very high UHI. But in July-Aug, the UHI rose clearly and many places became warmer. There were more orange and yellow spots, especially in central and southern parts. That month had the peak summer UHI in 2019. So, like in 2018, the middle summer month had the strongest heating (*Figure. 13*).

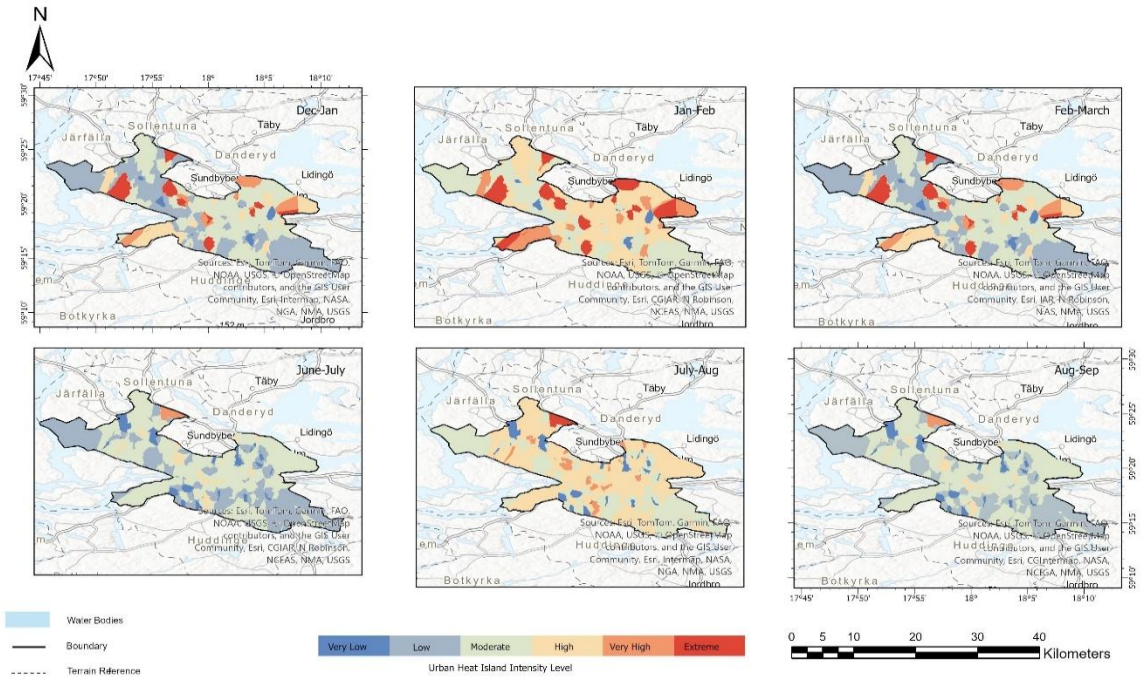

Figure. 13 UHI Intensity Map for 2019

In 2020, the winter months showed consistent and quite high UHI intensity throughout the whole season. Dec-Jan was the month where the UHI became stronger compared to the previous years, with large parts showing high UHI, especially in the central parts of the case

study. Jan-Feb followed with almost the same pattern. Most areas had moderate to extreme values, and only some few parts had low UHI. The whole city seemed to be affected more than usual. Feb-March continued with the same strength, and the pattern didn't change a lot. That winter had very strong UHI in general, and it was visible across all three months. In summer, Aug-Sept had the highest UHI of the three months, with many zones in the center and west showing high and very high UHI. Yellow and orange colors were more dominant in this map. July-Aug was the second hottest month in the summer, still showing high values but a bit less than August-September. June-July had the weakest UHI in 2020 summer, but still higher than the same period in some other years. In general, the summer in 2020 had overall higher UHI values than usual, and the central urban zones were the most affected (*Figure. 14*).

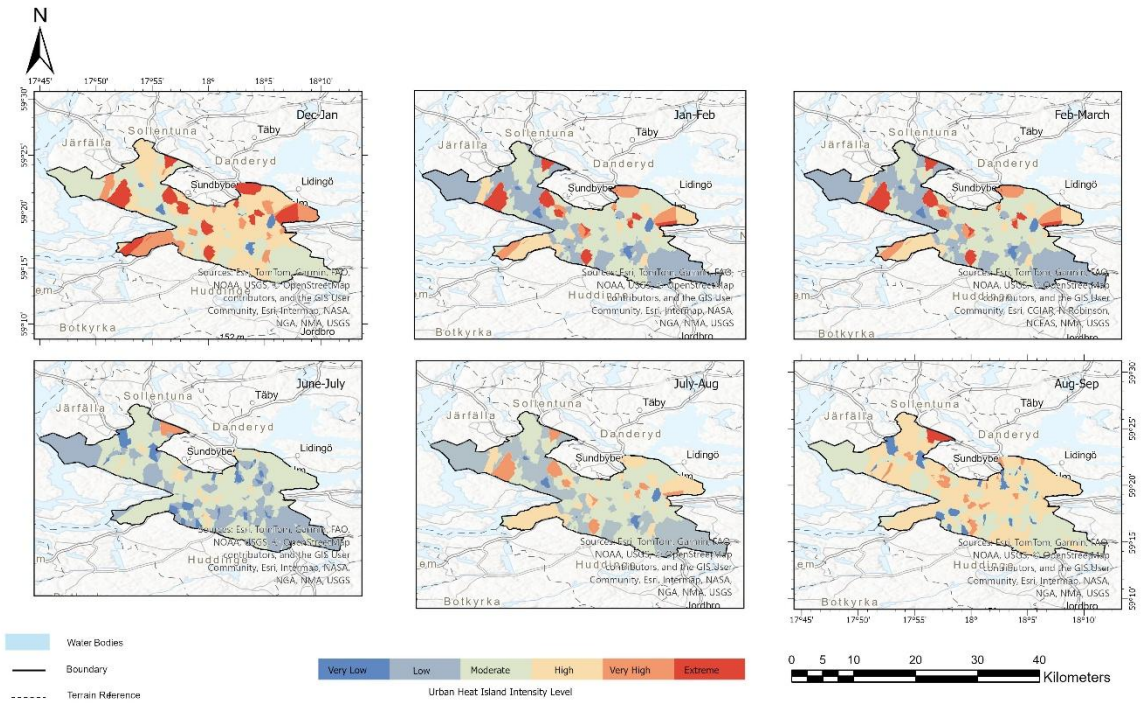

Figure. 14 UHI Intensity Map for 2020

UHI intensity in Stockholm showed distinct seasonal trends in 2021. During the summer the highest UHI were mainly "Low" to "Moderate", with the exception of Kista where "Very High" levels of UHI were observed. Kista is an urban region in north-western Stockholm where

the presence of impervious surfaces and lack vegetation might have intensified UHI. Conversely, areas bordering green spaces and water bodies recorded “Very Low” to “Low” levels. In the winter of 2021, overall UHI was more intense, particularly in central parts of the city and suburban areas with greater populations. At the same time, some urban areas still recorded “Very Low” to “Low” intensity. These results indicate that UHI persists during colder months (*Figure. 15*).

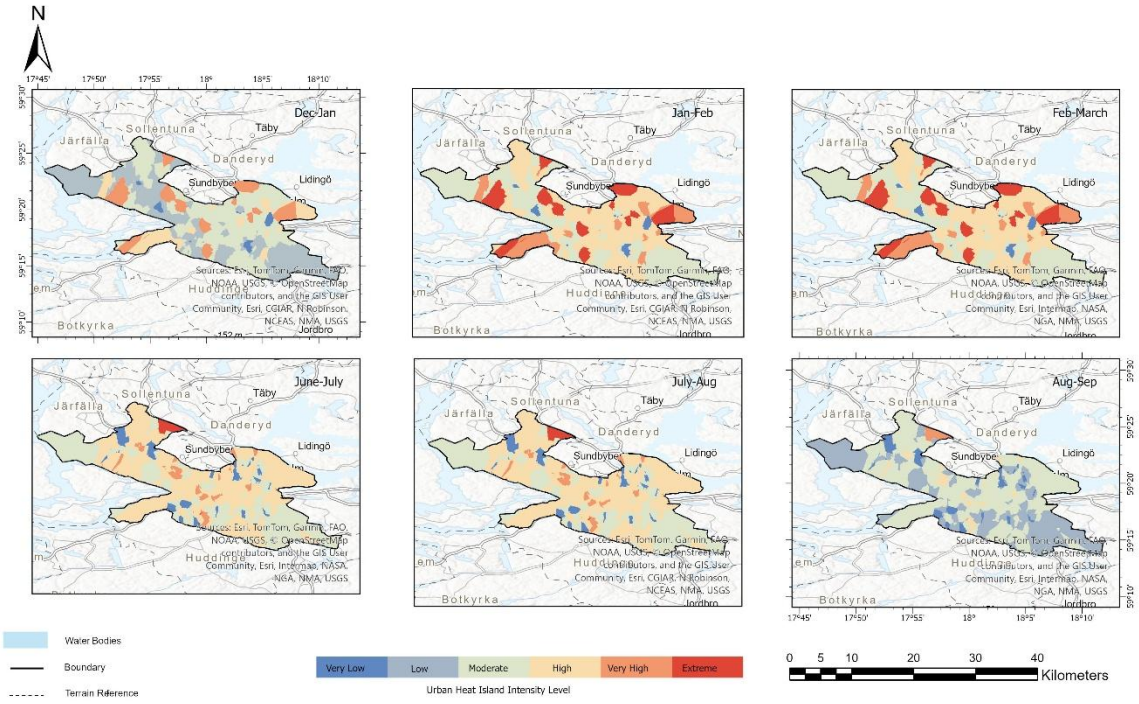

Figure. 15 UHI Intensity Map for 2021

The patterns for the summer of 2022 were similar to the previous year. However, areas with “Moderate” UHI intensity covered a larger portion of the city, likely due to higher temperatures or decreased vegetation coverage. Areas bordering green spaces and water bodies maintained “Low” UHI intensity, similar to 2021. In winter, UHI intensity was higher compared to 2022, but areas with “High” and “Extreme” intensities showed a broader distribution compared to 2021, suggesting that localized effects persisted (*Figure. 16*).

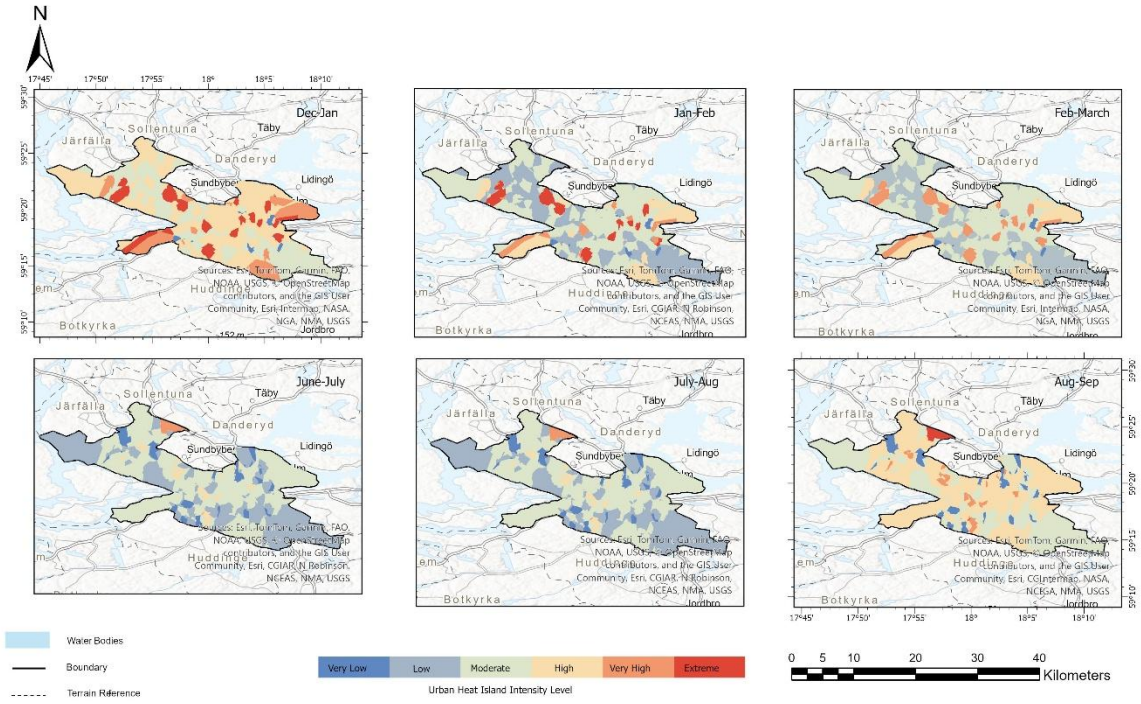

Figure. 16 UHI Intensity Map for 2022

In 2023, the winter showed some clear variation between the months. Feb-March had the highest UHI among the three winter months. Many areas in the central and northern parts had orange and red colors, meaning high and very high UHI. This was the peak winter month in terms of UHI. Dec-Jan had mostly moderate values, with a mix of yellow and green colors. It wasn't too low or too high, just stayed in the middle range. Jan-Feb had the lowest UHI, where a lot of parts of the case study were in light blue shades. That means the UHI effect was not strong during that period. In the summer, the result was a bit different than in previous years. Surprisingly, June-July had the highest UHI intensity. In this month, especially in the central areas of Stockholm, there were many yellow and even some orange spots. July-Aug and Aug-Sept followed with similar UHI shapes and moderate values. But it was clear that early summer was the hottest period in 2023, not the middle or end. The distribution stayed quite stable between the summer months, but the intensity was strongest in June-July (*Figure. 17*).

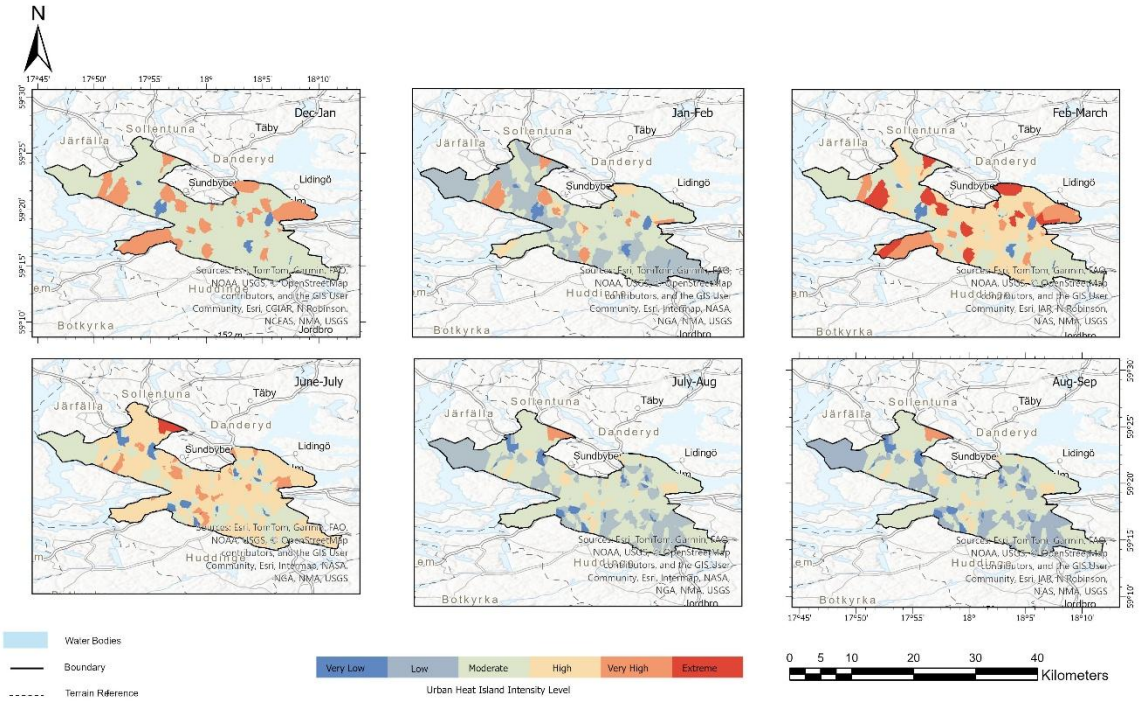

Figure. 17 UHI Intensity Map for 2023

For the temporal evolution analysis of UHI, the results showed a noticeable increase in UHI intensity, especially for the summer months. For instance, in some areas like dense build-up areas, which have impervious surfaces and low vegetation cover we have increased temperatures. Also, there are some interannual variability and the overall trajectory shows a increase of UHI over time.

With respect to LCZs, areas with higher building density in the city centre and those with larger populations experienced higher UHI intensity, likely reflecting the larger number of buildings, limited green spaces, and more surface area to absorb heat. LCZ 2 class (compact mid-rise) were most affected but UHI through the entire study period, showing moderate to very high UHI. Areas belong to LCZ 2 class are mainly located in central and eastern Stockholm, and rarely experience low UHI values.

LCZ 8 class, which is large low-rise: Large low-rise structures and is placed around north parts of the case study particularly, Kista, had also the most UH intensity between the LCZ classes.

This area known as one of the more populated areas in the case study. In most of the months and years, Kista showed very high and even extreme values of UHI, especially in winter seasons. Since LCZ 8 includes large structures with less ventilation and also more heat sources, it makes the area warmer. After LCZ 8, LCZ 6, which is open low-rise: low-rise buildings with open space class showed more UHI intensity in the area. These are the more suburban areas with some open space between buildings, but still not much greenery. UHI in these areas was mostly moderate to high in several periods, although sometimes they showed low values too, depending on the month.

On the other hand, LCZ A, dense trees: forests with high, continuous canopy cover class as expected showed the lowest UHI intensity for the study period with very low to low UHI intensity in most years in the study period. These areas are more natural, and located more outside of the built-up zones. Because they have more trees and shade, and also cooler surfaces, they usually didn't show any high UHI even during the summer months. Most of the time, LCZ A areas were blue or light blue in the maps, which means less heat. They were quite stable and consistent and didn't experience strong changes in UHI across the seasons.

4.3. Machine Learning Model Performance

With a 10-year dataset (using a total of 40,000 sample points and a 70-30 train-test split), multiple models were tested, and the results were obtained. *Table. 6* represents the results and performance of machine learning models, considering all the datasets.

Table. 6 Performance of different machine learning models

Models	**RMSE (°C)**	**R^2**	**MAE (°C)**
Linear Regression	6.7194	0.4045	5.6834
Ridge Regression	6.7194	0.4045	5.6834

Support Vector Regression (SVR)	5.5186	0.5983	3.1915
Decision Tree	0.8954	0.9894	0.3314
KNeighbors	4.9362	0.6786	2.8893
Random Forest	0.6527	0.9944	0.2566
Extra Trees	0.7382	0.9928	0.3332
XGBoost	0.6816	0.9939	0.2917

Tree based models (i.e., Random Forest, Extra Trees, and XGBoost) outperformed simple linear models. Overall, the Random Forest model exhibited the most consistent and robust performance due to their ability to capture non-linear relationships and complex interactions between multiple features, which are common in environmental and urban datasets, making it the ideal model across seasons and years due to its accuracy and stability.

The models also revealed the most important factors influencing UHI intensity. Random Forest and XGBoost were particularly remarkable in this regard, revealing the critical role of vegetation cover, impervious surfaces, and proximity to water bodies. The results suggest that expanding green areas and improving the design or urban environments can reduce UHI intensity the most severely affected areas. Such models are especially practical in areas with limited data and rapidly expanding urban areas. These models can infer general patterns and make generalization for unforeseen situations, making them a valuable tool under current and future conditions. Scenario-based modeling using these tree-based models enables policymakers and planners to base decision making on the predicted impacts of interventions, leading to more resilient and climate-aware urban planning.

4.4. Climate Change Projections Results

4.4.1. Projected UHI Trends for Winter (2030–2039)

For the SSP1-2.6, the results shows that the UHI value is increasing towards the year 2039, which shows a change in temperature in this scenario, which is a low emission and best scenario between climate change scenarios. In the first years of the projection, for example around 2030, the UHI value is estimated to be close to 1.12. But this value did not remain constant and showed a consistent increasing trend, reaching approximately 1.22 by the year 2039. This increase trend is not very high compared to the other scenario but yet shows a rise given the study area's current urban layout and population density. The steady rise in UHI under this scenario suggests that even moderate increases in temperature due to climate change can have a compounding effect on urban environments (*Figure. 19*).

With the worst-case scenario, scenario SSP5-8.5, the results of UHI are worse than before, for instance, in 2030, the projected UHI is already around 1.21. As the years progressed, the trend was upward, indicating a rise in urban heat intensity. By the year 2039, the UHI value had surged to approximately 1.27, showing a much more dramatic increase compared to SSP1-2.6 (*Figure. 18*). This sharp rise highlights the severe impacts that higher global warming scenarios can have on cities, especially when no significant mitigation strategies are implemented. The growing heat intensity in this scenario can potentially lead to more frequent and intense heatwaves, increased energy demand for cooling, and heightened risks for heat-related health problems, making it a serious concern for urban planners and policymakers.

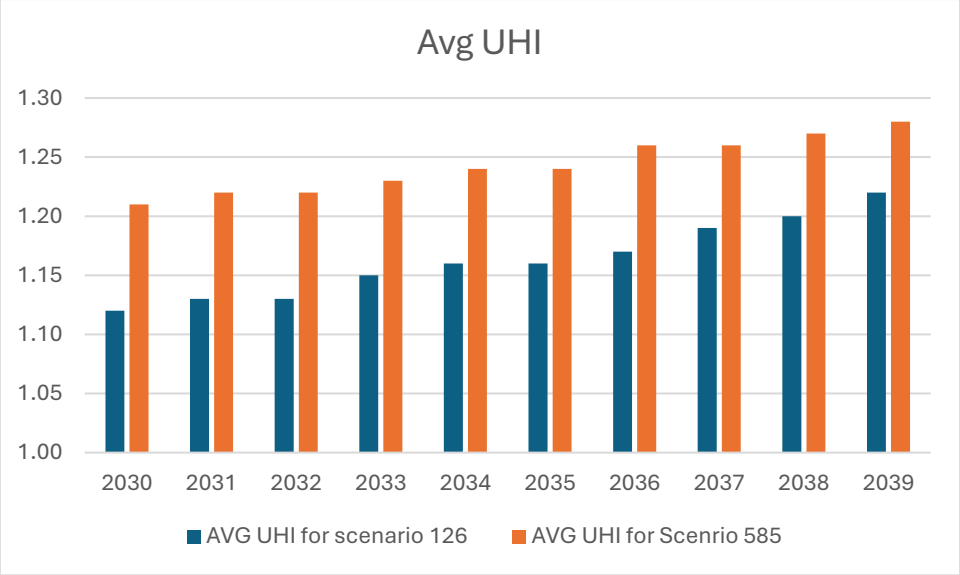

Figure. 18 UHI trend in winter under SSP1-2.6 and SSP5-8.5

4.4.2. Projected UHI Trends for Summer (2030–2039)

Under the SSP1-2.6 climate change scenario, an increasing trend was observed for 2030 to 2039, with higher values of UHI during summer months. The reason behind this event can be associated with higher weather temperature during the summer season. According to the obtained results, UHI intensity for the year 2030 was around 2.45, a high value for UHI, followed by an increasing trend in the following years, reaching to a value of 2.5 by the year 2039 (*Figure. 19*). This increase in UHI values can be associated with the land use change, urban expansion, and climate change impacts. This increasing trend underscores the thermal stress in cities, even in those with moderately controlled emission rates.

For the SSP5-8.5 scenario, the trend of projection also showed an increase of UHI intensity in the projection period. The projected UHI intensity in this scenario was of course more than the SSP1-2.6 scenario, since SSP5-8.5 scenario is the worst SSP scenario. For instance in the year 2030, the UHI showed a high value of around 2.5, which is a higher value compared to this year for SSP1-2.6 (*Figure. 20*). This trend of projection is increasing year by year making the summer 2039 the highest UHI intensity with around 2.6. Although the increase in the values

might seem not high, when considering this increase with some other variables and factors like humidity or other factors, the values can be considered significant.

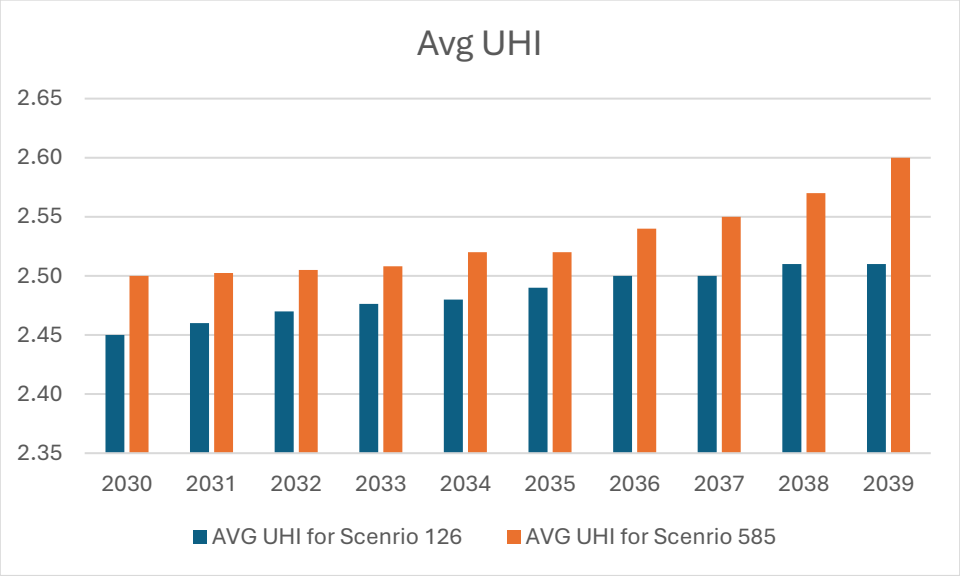

Figure. 19 UHI trend in summer under SSP1-2.6 and SSP5-8.5

5. Discussion

5.1. Interpretation of UHI Seasonal Trends

This study revealed the similarity in seasonal patterns across different years. Larger differences were observed between urban and rural areas during winter, particularly in January–February or in some cases December–January. The most affected areas remained the same across the year, including central Stockholm, Sundbyberg, and Kista, where there is dense development and limited green spaces.

A shift from low to moderate or high intensity levels of UHI was recorded in January-February of 2014, 2015, and 2016. During this time, some areas in the northeast and northwest of the city experienced moderate to high UHI, which is unusual since such intensities were not recorded in these areas even during summer.

Summer UHI patterns were different with regard to intensity and spatial and temporal distribution. Stockholm often experiences low to moderate levels of UHI in June, July, and August. “Very high” and “extreme” intensities are rare and mainly occur in small parts of the city centre. Spikes in UHI intensity can be observed in the middle of the summer (i.e., July and August), but this rise is significantly smaller in magnitude compared to similar events during winter; the clearest examples of this phenomenon occurred in two consecutive years: 2018 and 2019. It starts with low UHI intensity in June, followed by an increase the value of UHI in July and August. Finally in September the UHI intensity declines, and the cooling process begins. However, in 2020, this cycle was broken, showing higher UHI intensity in September and August in comparison to July. This pattern was observed in 2021 and 2022, as well.

The small gradual rise in UHI during summer (especially in August and September) from low to moderate levels appears to be independent of the annual UHI trend. This trend could be explained by urban development and general warming trends.

In general, the seasonal UHI patterns are consistent, characterized by higher levels in winter and lower levels in summer. However, more areas experience moderate UHI during summer. These observations underscore the importance of seasonal UHI analysis.

5.2. UHI in Cold Climate Cities

Literature review revealed that most studies on UHI have been conducted for case studies in warmer climates. However, studies which explore the UHI, its impacts on human well-being, energy use in colder climates are rare. The pattern of UHI in cities with colder climate like Stockholm is complex, making it require new pathways of strategy for heat management (Manoli et al., 2019).

The more intense UHI observed during winter can act as a buffer against extreme cold and offset energy cost and energy demand, particularly in highly-developed areas. Furthermore, warmer temperatures in urban areas can offer a level of protection for infrastructure against freeze-thaw cycles[4] by reducing frequency and intensity, leading to savings in maintenance and repair costs.

However, the negative impacts of UHI should not be overlooked, even in colder climates. The city centres in these regions are specially affected by heatwaves since there might be lack of green areas in these regions. These heatwaves can affect the people with health conditions or elderly people. When the heatwaves become more frequent because of climate change, cities in colder climates should be prepare for strategies to combat these events.

Overall, cold-climate cities such as Stockholm should strive to achieve a balance between the opportunities and challenges posed by UHI by developing methods to capitalize on the

[4] Freeze-thaw cycles occur when surfaces freeze overnight and thaw during the day, resulting in the damage of roads, sidewalks, and other infrastructure.

phenomenon during winter and combat its negative effects during summer. The positive and negative impacts of UHI in urban environments are summarized in Table 7.

Table. 7 Summary of UHI impacts

Potential Benefits of UHI (in cold climates)	Negative Impacts of UHI
Slight reduction in winter heating energy demand	Increased summer cooling demand
Reduced frost days in urban areas	Elevated risks of heat stress and mortality
Improved winter comfort in outdoor urban settings	Poor air quality due to trapped pollutants
	Accelerated climate change impacts in cities

5.3. Opportunities and Challenges of UHI in Winter

UHI can be beneficial during winter, particularly in colder climates. The captured heat in urban environments maintains ambient temperatures above the surrounding countryside, which could lead to a noticeable difference in cold cities such as Stockholm. Although this difference might seem small, it could lower the total heating energy expenditure over the course of the entire cold season, leading to economic savings and reduced environmental burden, especially since heating represents a large share of total energy use (Roxon et al., 2020).

Warmer temperatures during cold months also shield infrastructure (e.g., roads, bridges, pavements) against freeze-thaw cycles. Freeze-thaw cycles refers to temperature fluctuations around 0°C which lead to expansion-contraction of materials and repeated freezing and thawing of water. These repeated cycles of stress could shorted the life of infrastructure and increase repair, replacement, and maintenance costs. In areas affected by UHI during winter,

the conservation of heat reduces the number of these cycles, mitigating damage over time (Tan et al., 2023).

It is worth noting that overemphasizing the advantages of winter UHI and designing around its maximization could cause issues during warmer seasons. The same design principles which make heat capture possible in winter (e.g., heat-retaining materials and compact, low-ventilation layouts), prevent circulation and radiation of heat during summer, potentially worsening UHI. At the same time, interventions targeted at cooling during summer (e.g., reflective roofs and cool pavements) could lead to heat loss in winter. Therefore, a balance should be struck between heat preservation and exchange.

5.4. Green Infrastructure as a Mitigation Strategy

Green infrastructure has the unique advantage of offering benefits throughout the year. Tree canopies, green roofs, and urban parks provide cooling during summer by providing shade and absorbing heat via evapotranspiration. In winter, the same infrastructure offers insulation, reducing heat loss and energy demand (Leal Filho et al., 2021).

Venter et al., 2020 found out that vegetation cover can really affect and help to control UHI effects especially for areas with severe UHI in northern parts of Europe like Oslo, since vegetation cover can affect microclimates and consequently improving thermal comfort. Vegetation cover can also provide a good influence on health, which is a very good asset for urban design.

Every city faces unique challenges with respect to UHI, so the management strategies should be customized for each location to take into account climate, urban design, and energy use patterns. In Stockholm, an integrated approach should draw upon the current green spaces and incorporate innovative solutions to balance heat retention in winter and heat dissipation in summer.

6. Conclusion

The temporal and spatial pattern of UHI over the past 10 years was studied in this thesis. With the help of remote sensing and machine learning the UHI were analyzed and the results shows that dense, highly developed areas with limited vegetation were more affected by UHI during summer, while highly reflective areas with more extensive greenery maintained lower temperatures. Vegetation cover, studied using NDVI is one of the most important features for, also buildings, studied with the help of NDBI, was the most strongly associated variable with UHI. LSA and wind speed also played important roles in determining UHI patterns.

Between different LCZs, LCZ 2 class, which represents compact mid-rise and LCZ 8 class, which is large low-rise showed the most affected class of UHI through the entire study period, these areas are more populated and denser compared to other regions, while LCZ A, dense trees: forests with high, continuous canopy cover class as expected showed the lowest UHI intensity for the study period with very low to low UHI intensity in most years in the study period.

Several machine learning models were used in this study and the results showed that the Random Forest model was the best model because of the Random Forest ability to detect complex non-linear relationships and avoiding overfitting. The model outputs were highly accurate and offered insights into UHI dynamics. NDVI was the most influential variable once more, showing the important role of vegetation.

To ensure the accuracy and validate the UHI model, a 70-30 data split method is used and the results of the UHI analysis are compared and validated similar studies in Stockholm. Although the model can be used for other case studies as well, but it should be noted that the dataset with similar spatial resolution should be used.

There are some limitations in this study that need to be addressed. The first limitation is the coarse resolution of some data, for instance the CC projection models from NASA NEX-GDDP-CMIP6 are coarse and since in this thesis we work with higher resolution data, it makes the analysis more challenging. Also, there are some variables in this thesis, which are considered constant, which is not something that happens in the real world. These variables are NDVI, NDBI, LSA, and wind speed. Furthermore, some variables need to be considered for a more in-depth analysis of UHI, since this thesis is more focused on geophysical analysis, variables like population density or health impacts can be considered to have a more comprehensive analysis of UHI. Although the random forest showed the best results, using these results for an easy and understandable access could be challenging.

This works can be improved and expanded by incorporating projected urban development and land cover changes into the modelling process. Additionally, using more detailed climate data such as downscaled data or regional models can improve accuracy. Exploring the human dimensions of UHI such as demographics, socioeconomics, and health would also enrich future research by uncovering the most-affected populations. This research methodology could be used to assess the impacts of different mitigation strategies such as increased green spaces and reflective surfaces. Lastly, applying this framework to other cold-climate cities can elucidate whether the patterns observed in Stockholm are generalizable to other cities.

7. References

Alizadeh, M. J., Kavianpour, M. R., Kamranzad, B., and Etemad-Shahidi, A. (2019). A Weibull distribution based technique for downscaling of climatic wind field. Asia-Pacific Journal of Atmospheric Sciences, 55, 685-700.

Altman, N. S. (1992). An introduction to kernel and nearest-neighbor nonparametric regression. The American Statistician, 46(3), 175-185.

Arifwidodo, S. D., & Chandrasiri, O. (2020). Urban heat stress and human health in Bangkok, Thailand. *Environmental Research*, *185*, 109398.

Atkinson, B. W. (2003). Numerical modelling of urban heat-island intensity. *Boundary-Layer Meteorology*, *109*, 285-310.

Awad, M., Khanna, R., Awad, M., and Khanna, R. (2015). Support vector regression. *Efficient learning machines: Theories, concepts, and applications for engineers and system designers*, 67-80.

Breiman, L. (2001). Random forests. *Machine learning*, *45*, 5-32.

Breiman, L. (2017). *Classification and regression trees*. Routledge.

Chai, T., and Draxler, R. R. (2014). Root mean square error (RMSE) or mean absolute error (MAE)?–Arguments against avoiding RMSE in the literature. *Geoscientific model development*, *7*(3), 1247-1250.

Chen, T., and Guestrin, C. (2016, August). Xgboost: A scalable tree boosting system. In *Proceedings of the 22nd acm sigkdd international conference on knowledge discovery and data mining* (pp. 785-794).

Climate-Data.org. (n.d.). *Climate: Stockholm*. Retrieved January 28, 2025, from https://en.climate-data.org/europe/sweden/stockholms-laen/stockholm-196/

Cui, Y., Xu, X., Dong, J., & Qin, Y. (2016). Influence of urbanization factors on surface urban heat island intensity: A comparison of countries at different developmental phases. *Sustainability*, *8*(8), 706.

Danylo, O., See, L., Bechtel, B., Schepaschenko, D., & Fritz, S. (2020). Contributing to WUDAPT: A local climate zone classification of two cities in Ukraine. Urban Climate, 31, 100543.

Deilami, K., Kamruzzaman, M., and Liu, Y. (2018). Urban heat island effect: A systematic review of spatio-temporal factors, data, methods, and mitigation measures. *International journal of applied earth observation and geoinformation*, *67*, 30-42.

Demuzere, M., Bechtel, B., Middel, A., and Mills, G. (2019). Mapping Europe into local climate zones. PloS one, 14(4), e0214474.

Duhis, A. H., Aljanabi, M., & Al-Kafaji, M. S. S. (2023). Increasing photovoltaic system power output with white paint albedo–a scenario in Al-Mausaib City using PVSyst. software. *International Journal of Power Electronics and Drive Systems (IJPEDS)*, *14*(2), 1149-1159.

Dupuy, F., Durand, P., and Hedde, T. (2023). Downscaling of surface wind forecasts using convolutional neural networks. Nonlinear Processes in Geophysics, 30(4), 553-570.

Eliasson, I., & Holmer, B. (1990). Urban heat island circulation in Göteborg, Sweden. *Theoretical and Applied Climatology*, *42*, 187-196.

Estoque, R. C., Murayama, Y., & Myint, S. W. (2017). Effects of landscape composition and pattern on land surface temperature: An urban heat island study in the megacities of Southeast Asia. *Science of the Total Environment*, *577*, 349-359.

Fu, K., Ding, S., Zhang, L., Pan, M., Zhi, X., and Zhang, J. (2024, June). Deep Learning for Daily 10-m Wind Downscaling. In 2024 2nd International Conference on Mechatronics, IoT and Industrial Informatics (ICMIII) (pp. 146-150). IEEE.

González, S., García, S., Del Ser, J., Rokach, L., and Herrera, F. (2020). A practical tutorial on bagging and boosting based ensembles for machine learning: Algorithms, software tools, performance study, practical perspectives and opportunities. *Information Fusion*, *64*, 205-237.

Gonzalez-Trevizo, M. E., Martinez-Torres, K. E., Armendariz-Lopez, J. F., Santamouris, M., Bojorquez-Morales, G., & Luna-Leon, A. (2021). Research trends on environmental, energy and vulnerability impacts of Urban Heat Islands: An overview. *Energy and Buildings*, *246*, 111051.

Haine, K., & Blumberga, D. (2023, May). Exploring the Differential Effects of Urban Heat Islands on Energy Use and Carbon Emissions in Warm and Cold Climates: a Case Study of North Africa and North Europe. In *CONECT. International Scientific Conference of Environmental and Climate Technologies* (pp. 26-27).

Hatvani-Kovacs, G., Belusko, M., Pockett, J., & Boland, J. (2016). Assessment of heatwave impacts. *Procedia Engineering*, *169*, 316-323.

Heaviside, C., Macintyre, H., and Vardoulakis, S. (2017). The urban heat island: implications for health in a changing environment. *Current environmental health reports*, *4*, 296-305.

Hong, J. W., Hong, J., Kwon, E. E., & Yoon, D. K. (2019). Temporal dynamics of urban heat island correlated with the socio-economic development over the past half-century in Seoul, Korea. *Environmental Pollution*, *254*, 112934.

Howard, L. (1818). *The climate of London: deduced from meteorological observations, made at different places in the neighbourhood of the metropolis* (Vol. 1). W. Phillips, George Yard, Lombard Street, sold also by J. and A. Arch, Cornhill; Baldwin, Cradock, and Joy, and W. Bent, Paternoster Row; and J. Hatchard, Picadilly.

Huang, X., and Wang, Y. (2019). Investigating the effects of 3D urban morphology on the surface urban heat island effect in urban functional zones by using high-resolution remote sensing data: A case study of Wuhan, Central China. *ISPRS Journal of Photogrammetry and Remote Sensing*, *152*, 119-131.

Irfeey, A. M. M., Chau, H. W., Sumaiya, M. M. F., Wai, C. Y., Muttil, N., and Jamei, E. (2023). Sustainable mitigation strategies for urban heat island effects in urban areas. *Sustainability*, *15*(14), 10767.

Izenman, A. J. (2008). Modern multivariate statistical techniques (Vol. 1). New York: Springer.

Kerr, A., Rafuse, H., Sparkes, G., Hinchey, J., & Sandeman, H. (2011). Visible/infrared spectroscopy (VIRS) as a research tool in economic geology: background and pilot studies from Newfoundland and Labrador. *Geological Survey, Report*, *11*, 145-166.

Konstantinov, P., Varentsov, M., & Esau, I. (2018). A high density urban temperature network deployed in several cities of Eurasian Arctic. *Environmental Research Letters*, *13*(7), 075007.

Leal Filho, W., Wolf, F., Castro-Díaz, R., Li, C., Ojeh, V. N., Gutiérrez, N., ... and Bönecke, J. (2021). Addressing the urban heat islands effect: A cross-country assessment of the role of green infrastructure. *Sustainability*, *13*(2), 753.

Lialios-Bouwman, V., & Alstan Jakubiec, J. (2021, September). Urban heat islands in future climate scenarios. In *Building Simulation 2021* (Vol. 17, pp. 957-964). IBPSA.

Liang, S. (2001). Narrowband to broadband conversions of land surface albedo I: Algorithms. *Remote sensing of environment*, *76*(2), 213-238.

Liu, Y., Shen, C., Chen, X., Hong, Y., Fan, Q., Chan, P., ... and Lan, J. (2023). Satellite-Based Estimation of Roughness Length over Vegetated Surfaces and Its Utilization in WRF Simulations. Remote Sensing, 15(10), 2686.

Lum, C., Mackenzie, M., Shaw-Feather, C., Luker, E., & Dunbabin, M. (2016, July). Multispectral imaging and elevation mapping from an unmanned aerial system for precision agriculture applications. In *Proceedings of the 13th International Conference on Precision Agriculture* (Vol. 31, pp. 4-10).

Magli, S., Lodi, C., Lombroso, L., Muscio, A., and Teggi, S. (2015). Analysis of the urban heat island effects on building energy consumption. *International Journal of Energy and Environmental Engineering*, *6*, 91-99.

Manoli, G., Fatichi, S., Schläpfer, M., Yu, K., Crowther, T. W., Meili, N., ... and Bou-Zeid, E. (2019). Magnitude of urban heat islands largely explained by climate and population. *Nature*, *573*(7772), 55-60.

Marsh, C. B., Vionnet, V., and Pomeroy, J. W. (2023). Windmapper: An efficient wind downscaling method for hydrological models. Water Resources Research, 59(3), e2022WR032683.

Maulud, D., and Abdulazeez, A. M. (2020). A review on linear regression comprehensive in machine learning. *Journal of Applied Science and Technology Trends*, *1*(2), 140-147.

Meier, R., Davin, E. L., Bonan, G. B., Lawrence, D. M., Hu, X., Duveiller, G., ... and Seneviratne, S. I. (2022). Impacts of a revised surface roughness parameterization in the Community Land Model 5.1. Geoscientific Model Development, 15(6), 2365-2393.

Mohajerani, A., Bakaric, J., & Jeffrey-Bailey, T. (2017). The urban heat island effect, its causes, and mitigation, with reference to the thermal properties of asphalt concrete. *Journal of environmental management*, *197*, 522-538.

Nagelkerke, N. J. (1991). A note on a general definition of the coefficient of determination. *biometrika*, *78*(3), 691-692.

Nelli, N. R., Temimi, M., Fonseca, R. M., Weston, M. J., Thota, M. S., Valappil, V. K., ... and Al Naqbi, H. (2020). Impact of roughness length on WRF simulated land-atmosphere interactions over a hyper-arid region. Earth and Space Science, 7(6), e2020EA001165.

Oke, T. R. (1982). The energetic basis of the urban heat island. *Quarterly journal of the royal meteorological society*, *108*(455), 1-24.

Oke, T. R. (1988). Street design and urban canopy layer climate. *Energy and buildings*, *11*(1-3), 103-113.

Perera, N. G. R., & Emmanuel, R. (2018). A "Local Climate Zone" based approach to urban planning in Colombo, Sri Lanka. Urban Climate, 24, 178-188.

Qiu, C., Schmitt, M., Mou, L., Ghamisi, P., and Zhu, X. X. (2018). Feature importance analysis for local climate zone classification using a residual convolutional neural network with multi-source datasets. Remote Sensing, 10(10), 1572.

Quan, J., Ren, J., Du, Q., & Wang, D. (2018). Local Climate Zone mapping for urban sustainability: The case of Nanjing, China. Sustainability, 10(4), 1087.

Ren, C., Yang, R., Cheng, C., Xing, P., Fang, X., & Ng, E. (2020). Creating Local Climate Zone maps for urban planning in Chinese cities using an extended WUDAPT methodology: A case study of Guangzhou. Urban Climate, 31, 100545.

Rouse, J. W., Haas, R. H., Schell, J. A., and Deering, D. W. (1974). Monitoring vegetation systems in the Great Plains with ERTS. *NASA Spec. Publ*, *351*(1), 309.

Roxon, J., Ulm, F. J., and Pellenq, R. M. (2020). Urban heat island impact on state residential energy cost and CO2 emissions in the United States. *Urban Climate*, *31*, 100546.

Ryu, Y. H., & Baik, J. J. (2012). Quantitative analysis of factors contributing to urban heat island intensity. *Journal of Applied Meteorology and Climatology*, *51*(5), 842-854.

Salvati, A., Roura, H. C., & Cecere, C. (2017). Assessing the urban heat island and its energy impact on residential buildings in Mediterranean climate: Barcelona case study. *Energy and Buildings*, *146*, 38-54.

Sánchez-Guevara Sánchez, C., Núñez Peiró, M., & Neila González, F. J. (2017). Urban heat island and vulnerable population. The case of Madrid. *Sustainable Development and Renovation in Architecture, Urbanism and Engineering*, 3-13.

Sarrat, C., Lemonsu, A., Masson, V., and Guédalia, D. (2006). Impact of urban heat island on regional atmospheric pollution. *Atmospheric environment*, *40*(10), 1743-1758.

Solecki, W. D., Rosenzweig, C., Parshall, L., Pope, G., Clark, M., Cox, J., & Wiencke, M. (2005). Mitigation of the heat island effect in urban New Jersey. *Global Environmental Change Part B: Environmental Hazards*, *6*(1), 39-49.

Stewart, I. D. (2011). A systematic review and scientific critique of methodology in modern urban heat island literature. *International Journal of Climatology*, *31*(2), 200-217.

Stewart, I. D., & Oke, T. R. (2012). Local climate zones for urban temperature studies. Bulletin of the American Meteorological Society, 93(12), 1879–1900.

Statistics Sweden. (2023). *Statistics Sweden*. Retrieved January 28, 2025, from https://www.scb.se/en/

Suomi, J., & Meretoja, M. (2021). Trends and irregular variation of spatial temperature differences in the high-latitude coastal city of Turku, Finland. *Climate Research*, *84*, 41-57.

Sulaiman, M. A. (2020). Evaluating data mining classification methods performance in internet of things applications. *Journal of Soft Computing and Data Mining*, *1*(2), 11-25.

Svensson, M. K., & Eliasson, I. (2002). Diurnal air temperatures in built-up areas in relation to urban planning. *Landscape and urban planning*, *61*(1), 37-54.

Takkanon, P., & Chantarangul, P. (2019). Effects of urban geometry and green area on thermal condition of urban street canyons in Bangkok. *Architectural Science Review*, *62*(1), 35-46.

Tan, Y., Zhou, C., Zhong, C., and Zhou, J. (2023). Freeze–thaw and thermal cycle durability of pervious concrete with different aggregate sizes and water–cement ratios. *International Journal of Pavement Engineering*, *24*(2), 2021405.

Tang, B. H., and Bassill, N. P. (2018). Point downscaling of surface wind speed for forecast applications. Journal of Applied Meteorology and Climatology, 57(3), 659-674.

Trepekli, K., and Friborg, T. (2021). Deriving aerodynamic roughness length at ultra-high resolution in agricultural areas using UAV-borne LiDAR. Remote Sensing, 13(17), 3538.

Vapnik, V. (1995). Support-vector networks. *Machine learning*, *20*, 273-297.

Venter, Z. S., Krog, N. H., and Barton, D. N. (2020). Linking green infrastructure to urban heat and human health risk mitigation in Oslo, Norway. *Science of the Total Environment*, *709*, 136193.

Voogt, J. A., and Oke, T. R. (2003). Thermal remote sensing of urban climates. *Remote sensing of environment*, *86*(3), 370-384.

Werner, J. (2023). Accessibility of green spaces with recreational values: A GIS network analysis for the City of Stockholm.

Willmott, C. J., and Matsuura, K. (2005). Advantages of the mean absolute error (MAE) over the root mean square error (RMSE) in assessing average model performance. *Climate research*, *30*(1), 79-82.

Wong, N. H., Tan, C. L., Kolokotsa, D. D., & Takebayashi, H. (2021). Greenery as a mitigation and adaptation strategy to urban heat. *Nature Reviews Earth & Environment*, *2*(3), 166-181.

Xu, M., Watanachaturaporn, P., Varshney, P. K., & Arora, M. K. (2005). Decision tree regression for soft classification of remote sensing data. Remote Sensing of Environment, 97(3), 322-336.

Xu, X., González, J. E., Shen, S., Miao, S., & Dou, J. (2018). Impacts of urbanization and air pollution on building energy demands—Beijing case study. *Applied Energy*, *225*, 98-109.

Zha, Y., Gao, J., and Ni, S. (2003). Use of normalized difference built-up index in automatically mapping urban areas from TM imagery. *International Journal of Remote Sensing*.

Zhou, Y., Wei, T., Zhu, X., and Collin, M. (2021). A parcel-based deep-learning classification to map local climate zones from sentinel-2 images. IEEE Journal of Selected Topics in Applied Earth Observations and Remote Sensing, 14, 4194-4204.

8. Appendix

Table of Figures